

DOCUMENT SIGNATURE PAGE

	Name & Function	Date	Signature
Prepared by:	<i>A. Hahne</i> <i>ESA/SSST</i>	<i>19/11/</i> <i>2011</i>	<i>A. Hahne</i>
Approved by:	<i>ESA</i> <i>Programme Manager</i>		
Approved by:	<i>EUMETSAT</i> <i>Programme Manager</i>		

Table of Contents

1	Introduction	5
1.1	Statement of the problem	5
1.2	Purpose and Scope	5
2	Reference documents	5
3	Observations	6
3.1	General observation during operational mode	6
3.2	Design related aspects concerning the in-orbit observations	16
3.2.1	LEDs compared to other sources	16
3.2.2	FPA compared to PMD	17
3.3	Complementary observations during specific in-orbit events	18
3.3.1	Switch-offs of the instrument	18
3.3.2	First throughput test	20
3.3.3	Second throughput test	22
4	Facts, OBSERVATIONS, INITIAL conclusions	27
4.1	LED Records	27
4.2	White Light Source versus Sun Records	27
4.3	Scan Mirror Degradation	28
4.4	Optics degradation	29
4.5	Dynamics during TT2	29
5	Deduced properties of a deposit	30
6	Finding the candidate material	30
7	Building the hypothesis	34
7.1	The Spaces Involved	34
7.2	Steady State Hypothesis	41
8	Discussion	44
8.1	Spectral Features	
8.2	Temperature dependence of signal during TT1/TT2	
8.3	Evolution of the FWHM	
9	Summary and Conclusion	50
10	Appendix	52

1 INTRODUCTION

This document is a re-issue of the document EUM/LEO/REP/09/0732 to formally endorse the final report of the investigation group.

1.1 Statement of the problem

A continuous throughput degradation has been observed on the GOME-2 FM3, a UV-VIS spectrometer onboard Metop-A. The signal at the output of the instrument decreased with a spectral signature: the losses are around 20 %/year in the UV part of the spectra and 10 %/year in the visible. These losses have been estimated as the linear annual rate of degradation since the beginning of life.

This leads to the degradation of the products and, in a long-term frame, possibly to the loss of the operational status of the some products. Up to now the quality of all the operational products is within the specifications.

Investigations are being performed in order to understand the phenomenon and to define possible actions for mitigating the on-going degradation and/or for avoiding the same problem on the Metop-B and C satellites.

1.2 Purpose and Scope

This document summarises:

- the observations relevant for the investigation on the throughput loss
- the possible hypotheses and causes for the throughput loss

At this point of time, the purpose of the document is to gather and exchange the relevant information about the throughput loss. It will provide a frame to discuss the interpretation of the observations and the consistency of the theories elaborated to explain the throughput degradation.

2 REFERENCE DOCUMENTS

- [RD1] GOME Annual In-Flight Performance Report 2009, EUM/OPS/DOC/09/1092
- [RD2] GOME-2 FM3 long-term in-orbit degradation - status after 1st throughput test, EUM/OPS-EPS/TEN/08/0588
- [RD3] GOME-2 FM3 Long-Term In-Orbit Degradation - Status After 2nd Throughput Test, EUM/OPS-EPS/TEN/09/0318
- [RD4] Support for Analysis of GOME-2 In-Orbit Degradation and Impact on Level 2 Data Products, EUM/MET/SOW/09/0311
- [RD5] GOME-2 FM3 long-term in-orbit QTH lamp blackening – analysis, test proposal and mitigating action plan, EUM/OPS/TEN/09/1504
- [RD6] GOME2 Design Specification, MO-DS-GAL-GO-0003
- [RD7] Temperature Dependence of Spectral Characteristics of Silicon Photodiodes in the Ultraviolet Region, L.S. Lovinskii, Izmeritel'naya Tekhnika, No. 11, pp. 26-27, November, 2000
- [RD8] GOME-2 L1 Product Generation Specification, EPS.SYS.SPE.990011, v6.1
- [RD9] TRR-B for 2nd GOME-2 instrument throughput test, EUM/OPS-EPS/MIN/09/0343, v1.
- [RD10] Thruster plume impingement description report, MO.NT.MMT.SY.0075
- [RD11] 20 N Hydrazine Thruster Plume effects on GOME

3 OBSERVATIONS

This section gives an overview of the problem through the different observations made during normal operation and specific events and tests.

3.1 General observation during operational mode

The throughput of GOME-2 is monitored looking at the instrument output in response to an incoming signal assumed to be stable with time. The signals used for this are:

- The sun reflected by a diffuser (solar mean reference (SMR) measurement mode)
- The white light source (WLS)
- An ETALON residual effect derived from WLS measurements
- The spectral light source (SLS)
- The SLS Over Diffuser (SLSDif)
- Moon Calibrations
- Earth measurements over stable areas –e.g. Sahara
- The LEDs which are inside the optical path, in the vicinity of the detectors

Table 3-1 lists the processing or calibration steps that have been applied to the individual signals used for throughput monitoring.

Monitoring Source	Calibration/processing steps	[units]
LED	<ul style="list-style-type: none"> • Dark offset subtracted for given temperature and integration time • Normalised to seconds 	[BU ¹ /sec]
SLS/SLSDif	<ul style="list-style-type: none"> • Dark offset subtracted for given temperature and integration time • Pixel to Pixel gain offset subtracted • Normalised to seconds 	[BU/sec]
WLS	<ul style="list-style-type: none"> • Dark offset subtracted for given temperature and integration time • Pixel to Pixel gain offset subtracted • Normalised to seconds • <i>Corrected for Etalon effect²</i> 	[BU/sec]
ETALON	Relative change of overall instrument etalon with respect to an etalon measured on ground and using the	[-]

¹ Photo-electron counts in binary units BU

² This calibration step has been added for WLS only for throughput monitoring purposes and is not used during the operational level 0 to 1B processing.

	<p>WLS signal (calibrated as before without etalon correction and at a given temperature). No change w.r.t. the pre-launch situation would therefore result in 1 for all detector pixels per channel.</p>	
SMR	<ul style="list-style-type: none">• Dark offset subtracted for given temperature and integration time• Pixel to Pixel gain offset subtracted• Normalised to seconds• Corrected for Etalon effect• Corrected for Stray-light• Calibrated for irradiance response• Doppler shift correction	[photons/(sec nm cm ²)]

Earthshine/Moon	<ul style="list-style-type: none"> • Dark offset subtracted for given temperature and integration time • Pixel to Pixel gain offset subtracted • Normalised to seconds • Corrected for Etalon effect • Corrected for Stray-light • Calibrated for radiance response 	[photons/(sec nm cm ² sr)]
-----------------	---	---------------------------------------

Table 3-1: List of calibration steps applied for the various signals used for the throughput analysis. Note that all calibration steps are always acquired at the same temperature and for a given valid integration time (w.r.t. dark measurement). Otherwise they are not considered as being valid and not used. Note also that in most cases the presented time series are normalised to a certain reference time and the result is therefore dimensionless.

The differences between the optical paths from the light sources bring complementary information to locate the component involved in the throughput loss.

Since the beginning of its orbit life, the GOME-2 instrument has shown a steady degradation of its throughput especially in the UV domain.

The following plots show the throughput evolution derived from the different light source signals at selected wavelengths representative of each of the four FPA channels.

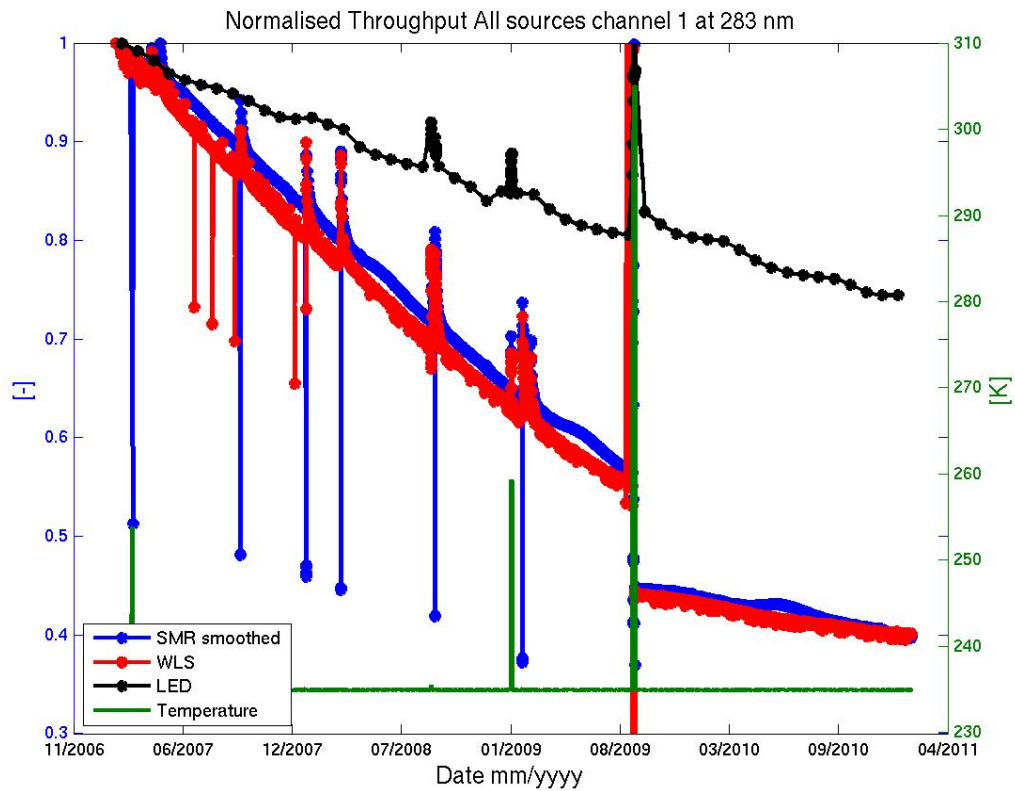


Figure 3-1: Change in instrument throughput at 283. SMR (blue line), WLS (red line) and LED (black line). Note that LEDs illuminate at 570 nm over the whole detectors. LED measurements are only made once per month. The data have been normalised to an average over the first 412 orbits (29 days) starting 20 January 2007.

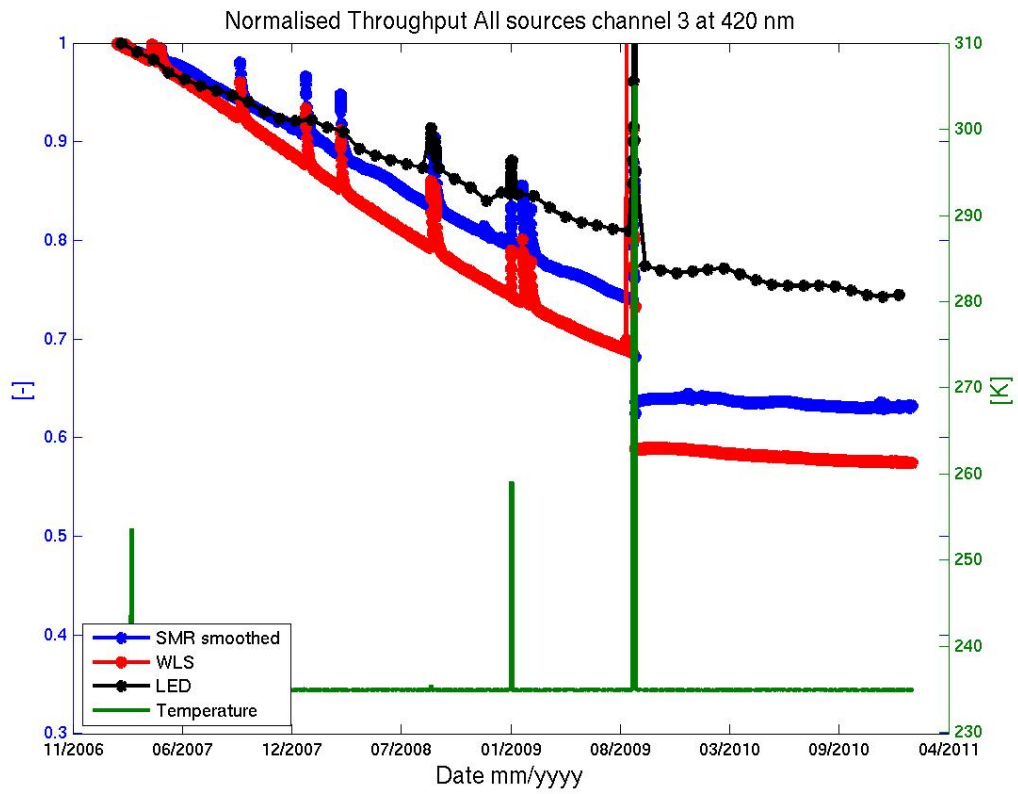


Figure 3-2: Same as Figure 3-1 but for channel 2 at 420 nm

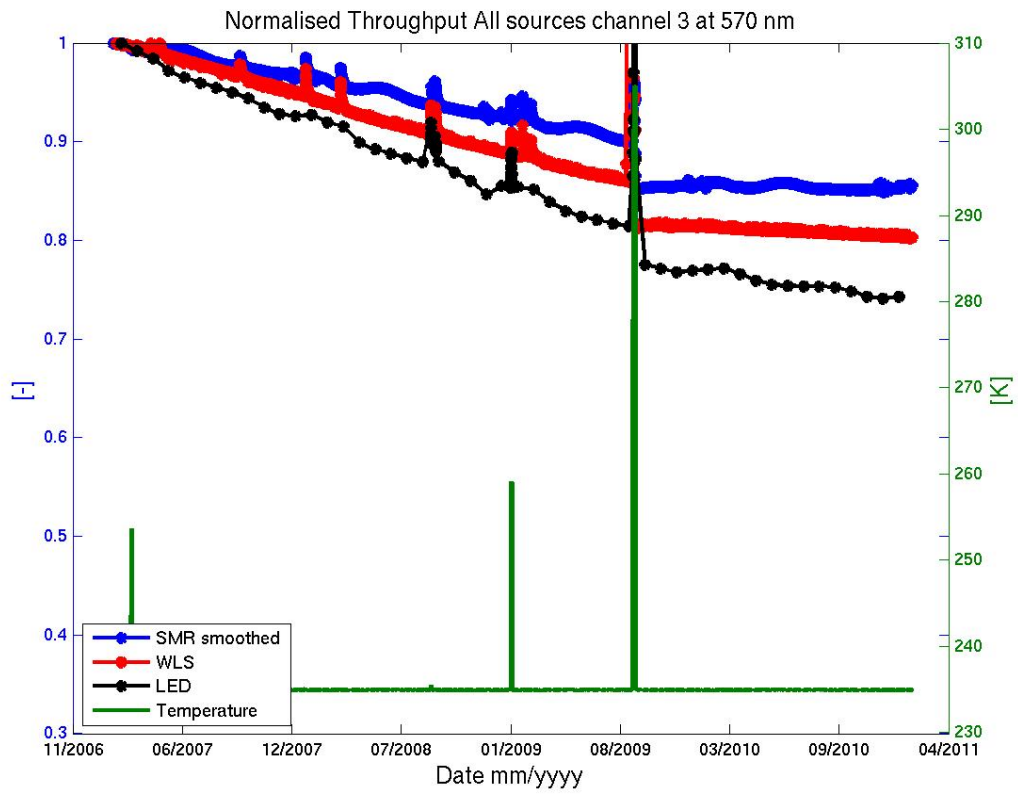


Figure 3-3: Same as Figure 3-1 but for channel 3 at 570 nm

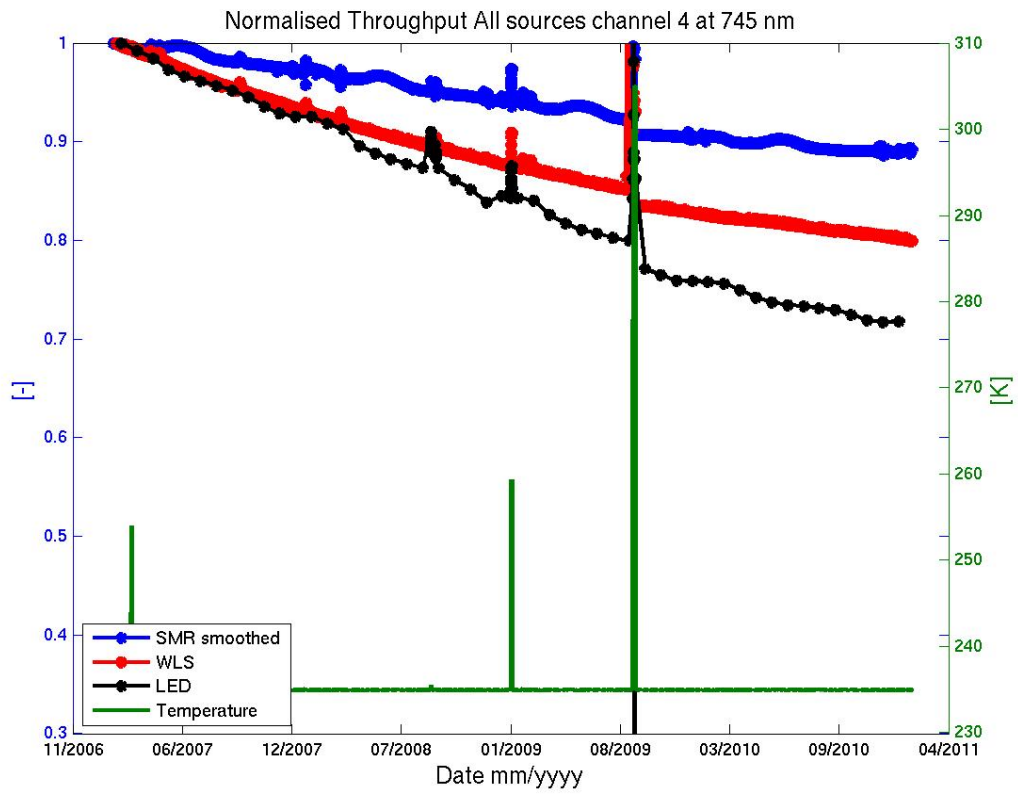


Figure 3-4: Same as Figure 3-1 but for channel 4 at 745 nm

The linear degradation rate (with respect to beginning 2007) before the second throughput test in September 2009 is given for each channel and for each light source in Table 3-2 and graphically represented on Figure 3-5. The degradation rate after the second throughput test is shown in Table 3-3 and Figure 3-6.

Channel (wavelength)	WLS	SMR	LED
1 @ 283 nm	-18 %/year	-18 %/year	-8 %/year
2 @ 420 nm	-13 %/year	-11 %/year	-8 %/year
3 @ 570 nm	-6 %/year	-4 %/year	-9 %/year
4 @ 745 nm	-6 %/year	-3 %/year	-8 %/year

Table 3-2: Annual degradation rate of the different spectral channels measured thanks to the different light sources before the second throughput test

Channel (wavelength)	WLS	SMR	LED
1 @ 283 nm	-3 %/year	-3 %/year	-7 %/year
2 @ 420 nm	-1 %/year	-1 %/year	-3 %/year
3 @ 570 nm	-1 %/year	0 %/year	-3 %/year
4 @ 745 nm	-3 %/year	-1 %/year	-4 %/year

Table 3-3: Annual degradation rate test of the different spectral channels measured thanks to the different light sources after the second throughput

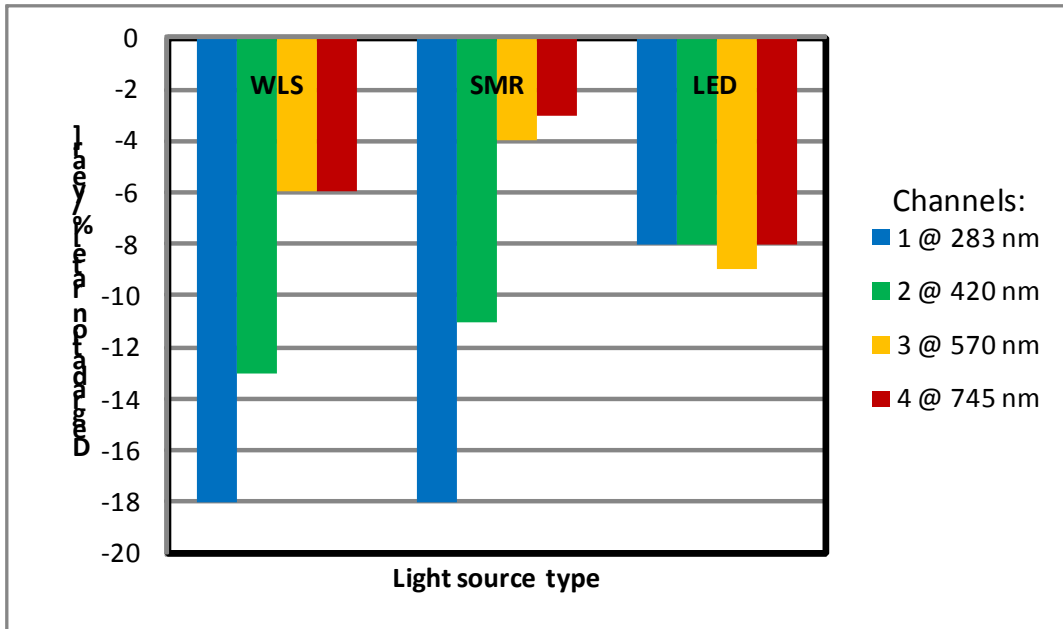


Figure 3-5: Throughput degradation rate measured thanks to the various light sources before the second throughput test

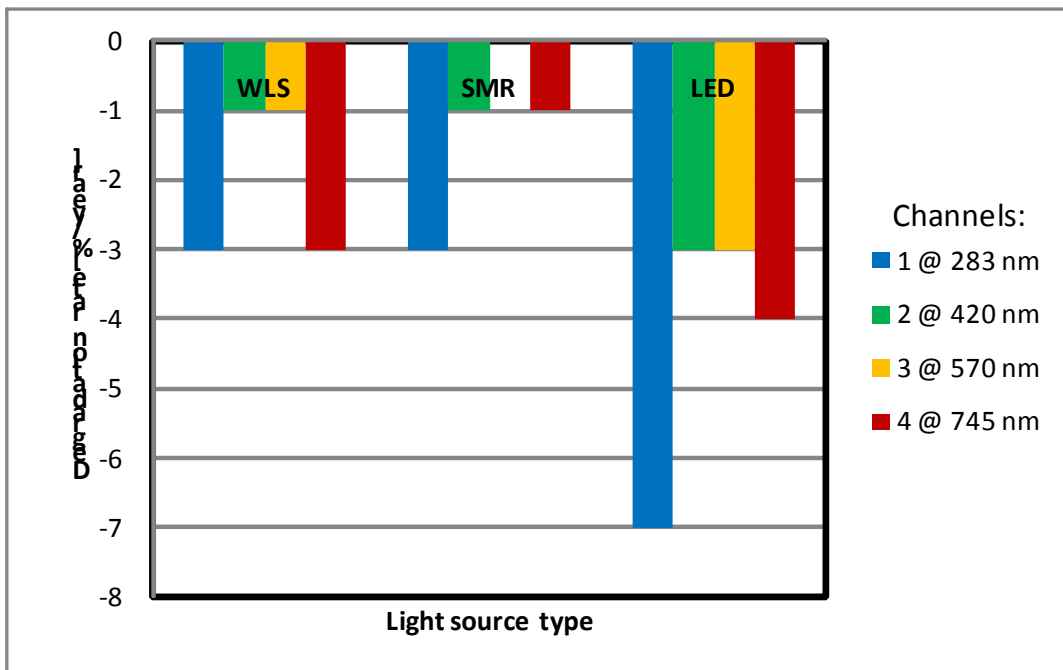


Figure 3-6: Throughput degradation rate measured thanks to the various light sources after the second throughput test

First, it can be seen that the losses are spectrally dependant: **the throughput degradation is larger in the short wavelengths especially in the UV range.**

On the other hand, discrepancies can be noted between the results provided by the different light sources. This could be explained by the difference of optical path between the sources and by aging of the sources.

Nevertheless, the general trend remains a **throughput loss with a strong spectral dependence for both the FPAs and the Polarisation Monitoring Devices (PMD).**

A calibration parameter called the **etalon** is also monitored in the frame of the throughput degradation. The etalon is a measurement of the spectrally dependent bias in signal due to the instrument optics. The residual etalon effect with respect to the on-ground calibrated overall etalon of the instrument is removed during the GOME-2 level 0 to 1b data processing. This residual etalon, expected to show moderate long and short term variations during the instrument lifetime, is derived from the on-board white light source WLS. Results of the long-term behaviour of this residual etalon are shown in the following (Figure 3-7).

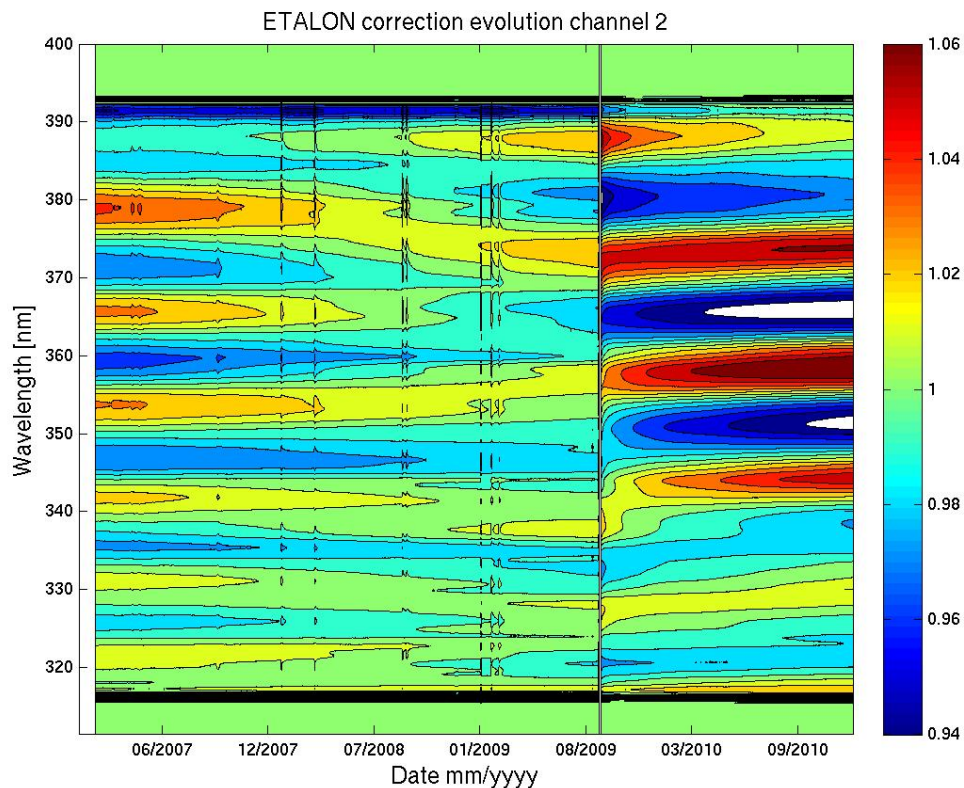


Figure 3-7: Residual etalon evolution for channel 2

A study to assess the **impact of the throughput degradation on the level 2 products** is being performed [RD4]. The first results are expected by January 2011. The final report of this study is due for May 2011.

3.2 Design related aspects concerning the in-orbit observations

The discrepancies between the different kinds of observation may be related to the instrumental design. They can be representative of the differences between the light paths from the sources to the detectors. These discrepancies can therefore help to discriminate the influence of the different components of the instrument.

The main components of the optical path are (from the entrance to the detectors):

- The scanning mirror and the telescope
- The calibration unit and in particular the diffuser (for solar path only)
- The pre-disperser prism
- The beam-splitters
- The gratings
- The focusing objectives
- The detectors

An artist impression of the optical layout is given in appendix, .

The refractive elements are made in fused silica (Suprasil type). The optical coatings are made in MgF₂, but the detailed design is proprietary by the suppliers.

The observations presented in the previous section are now interpreted in light of the instrumental design.

3.2.1 LEDs compared to other sources

By design, the LEDs are located close to the detectors. More precisely they are set inside the focusing objectives in front of a second group of lenses. The remaining optical path from the LEDs to the detectors is:

- A couple of lenses
- The entrance windows of the box of the detectors (only for the FPA)
- The detectors

Each Focal Plane Assembly (FPA) detector is located in its own enclosed box. Therefore the FPA are isolated from the rest of the instrument. The FPA detector boxes are connected to the outside environment thanks to narrow exhaust pipes. The exhaust pipes have a common external side located outside the instrument box, under the MLI.

The LEDs allow the monitoring of the detectors, specifically and independently from the upstream optical path.

The differences between the losses observed with the LEDs and on the other hand with the other light sources can be explained by the spectral emission of the LEDs and their location in the vicinity of the detectors.

First, the LEDs emit only around 570 nm. The measurements made thanks to the LEDs should therefore be compared only to the losses observed in the channel 3 because of the observed spectral dependence of the degradation. If this is done (Figure 3-3 and Table 3-2), the same range of loss is observed: around 8 %/year. The measurements of Table 3-2 have been interpolated to deduce the loss rate at 500 nm (– 8 %/year for the WLS, – 7 %/year for the SMR and – 9 %/year for the SLS). On the other hand, the optical path is shorter for the LEDs with less optical components (likely to degrade).

The consistency between the LED measurements from a channel to another suggests that at least a part of the green light degradation **is affecting all the channels in roughly the same way**. The common degradations measured for all the light sources in channel 3 can be interpreted as the fact that:

- **This part of the observed degradation is instrumental degradation and not light source degradation** (the probability that all the sources experience the same degradation is low)
- **This part of the degradation problem is located in the remaining optical path after the LEDs**. Therefore the detection chain may be an important component of the throughput degradation.

3.2.2 FPA compared to PMD

In spite of the fact the PMD and FPA are contained in very different environments they exhibit broadly speaking the same degradation rate both in time and spectral space. Figure 3-8 shows the long term signal variation for both PMDs and the FPA at 310 nm.

The optical path for the PMD is different from the one for the FPA except for the scan mirror and the telescope. After the first pre-disperser prism, the FPA path and the PMD path are distinct. The PMD spectra are obtained thanks to prisms instead of gratings for the FPA. The detector designs are also different: the FPA detectors are enclosed in their own boxes whereas the PMD detectors are not isolated from the optical bench environment.

In spite of the broadly similar degradation of PMD and FPA there are also differences observed on smaller scales, which are worth mentioning.

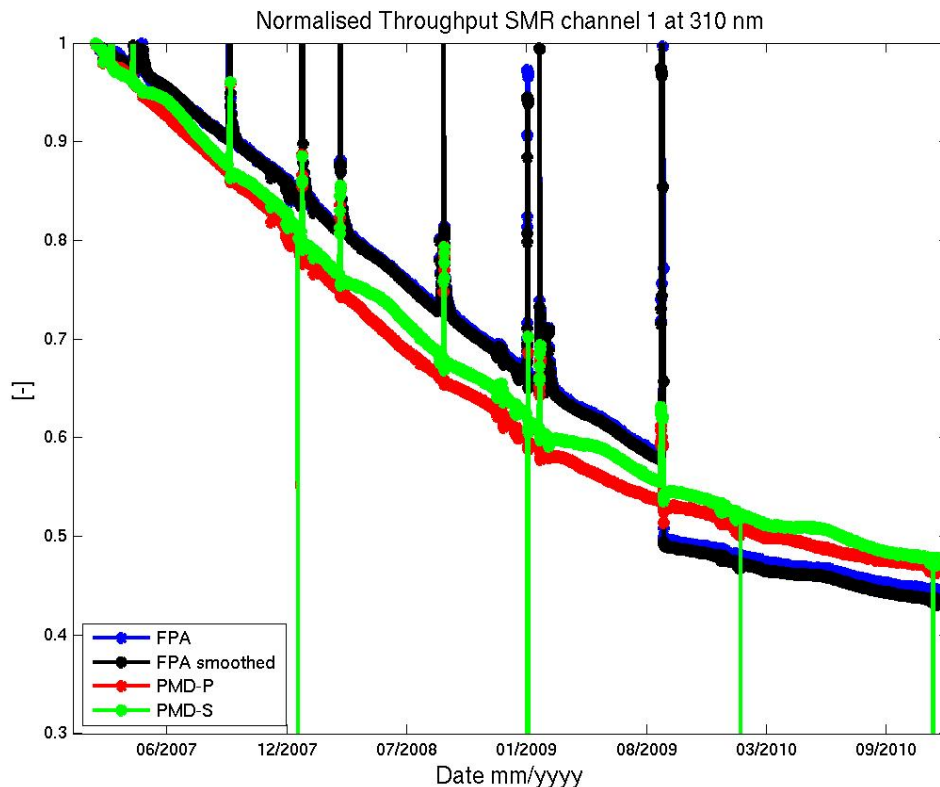


Figure 3-8: SMR long term evolution for the both PMDs and the FPA at 310 nm. The plot FPA smoothed corresponds to the FPA convoluted to the PMD spectral response

To complement the observations provided by the instrument in operational mode, dedicated in-orbit tests have been performed. Specific events such as instrument switch-offs were also considered to improve the understanding of the throughput loss.

3.3 Complementary observations during specific in-orbit events

Three different events are discussed here:

1. The switch-offs of the instrument consecutive of PLSOL or EQSOL (two switch-offs occurred for example in September 2008)
2. The first throughput test performed end of January 2009
3. The second throughput test performed in September 2009

3.3.1 Switch-offs of the instrument

3.3.1.1 Observations

During GOME-2 instrument switch-offs, the cooling system for the detectors is switched off and the instrument cools down significantly overall. However a survival heater is enabled to stop the FPAs becoming too cold such that the detector temperature may become warmer than the environment temperature, depending on the duration of the switch-off.

The thermal state of the optical bench is affected during a switch-off. There is an overall cooling effect due to equipment such as coolers, Scan Unit etc dissipating less power. The Optical Bench Temperatures drop by approx 20 K from 278 K to 258 K.

In the absence of cooling, the FPA detectors rise from their nominal 238 K to approx 255 K (with a +/- 2 K orbital variation). The FPAs are connected to the radiator and kept warm by an externally powered survival heater which is automatically activated by the closing of a mono-stable relay at switch-off.

The PMD detectors rise from approx 232 K to 257 K.

After a switch-off, the throughput of the FPAs is increased compared to the previous state before the switch-off. These events are visible on the plots (Figure 3-1 to Figure 3-4): spikes appear on the curves. Then, within a time period of around **10 days** the throughput of the FPAs returns to the previous state of degradation following a kind of damped mode. Such hysteresis behaviour is not observed for the PMDs which return to the previous throughput state in few hours.

Figure 3-9 shows the evolution of the throughput of FPA channel 3 measured by the SMR and the LEDs during the two subsequent switch-offs in September 2008 (on-board software patch). The general shape is indeed a spike followed by hysteresis behaviour.

Shortly after the first switch-off LED measurements were made on 5 successive orbits, followed by daily SMR measurements. The SMR curve takes over where the LED curve left off. During the second switch-off, the SMR and LED measurement were alternated during a few orbits, followed by daily SMR measurements. On this second switch off, the initial SMR signal appears to have recovered less than the LED signal.

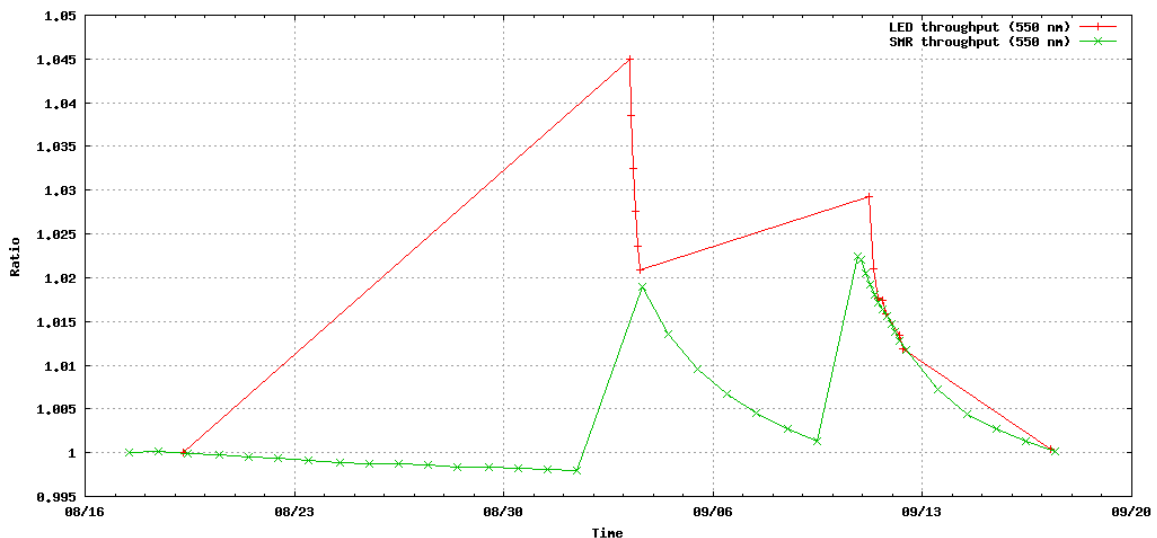


Figure 3-9 GOME-2 FPA throughput at 550nm for LED (red line) and SMR (green line)

The fact that the throughput recovery is also seen by the LEDs suggests that the FPA are directly affected by the switch-offs in such a way that the throughput is increased. Moreover

the lower recovery seen thanks to the SMR could be explained by the uncertainty on the emission wavelength of the LEDs or by some additional degradation in the optical path before the LEDs. This additional degradation would not be affected by the switch-off.

The PMD throughput in contrast shows a different behaviour: their throughput is increased shortly after a switch-off but it comes back to its previous level quasi instantaneously when the PMD detector temperature is set to its operational value) needs further investigation.

The different behaviour of the FPA/PMD throughput in the context of instrument switch-offs needs further investigations.

Very small residual etalon changes before and after the switch-offs have been observed. The exact time-scale of which has to be investigated.

The throughput increase consecutive to the switch-offs of the GOME-2 instrument leads to the assumption of a contamination of the detectors which may be partly removed (evaporation) by an increase of the detector temperature however at very different time scales for PMD and FPAs.

3.3.2 First throughput test

Based on the recovery observed during the switch-offs a specific test has been set up. It was carried out the 27th to the 29th January 2009.

The test mainly consists in increasing the temperature of the detectors in order to increase the throughput by removing the assumed contaminants. This way, thermal conditions similar to those during a switch-off are reproduced. Note that the major differences between a test and a real switch-off are:

- 1- The instrument temperature during the test is larger than during a switch-off because the instrument is switched on, and dissipates energy. The optical bench temperature is 276 K during the test whereas it is assumed to be around 258 K during GOME-2 switch-off periods.
- 2- During switch-off a survival heating process is activated. A dale resistor is automatically closed when a switch-off occurs. This resistor warms the backplates of the FPA detectors which are thermally coupled to the radiator. During the throughput test the dale resistor is maintained opened.

3.3.2.1 Experimental protocol

For the first throughput test, the FPA temperature was increased with 5 K steps from nominal temperature (235 K) up to 265 K. Each step lasted for 3 orbits. The PMD temperature cannot be controlled in such a precise way. Only 3 working modes are available for the PMD coolers: FlightLine, GroundLine and Off. The PMD Peltier coolers were set in GroundLine (low power) mode for the test. They reach a temperature of 268 ± 2 K, then change according to the power output by the FPA coolers.

3.3.2.2 Observations

During the first throughput test, the temperature of the FPA follows the commands (Figure 3-10) except for the highest temperatures. This can be explained because the Peltier coolers of the FPA were not used in heating mode, which prevents from reaching temperatures higher than the temperature of the surroundings.

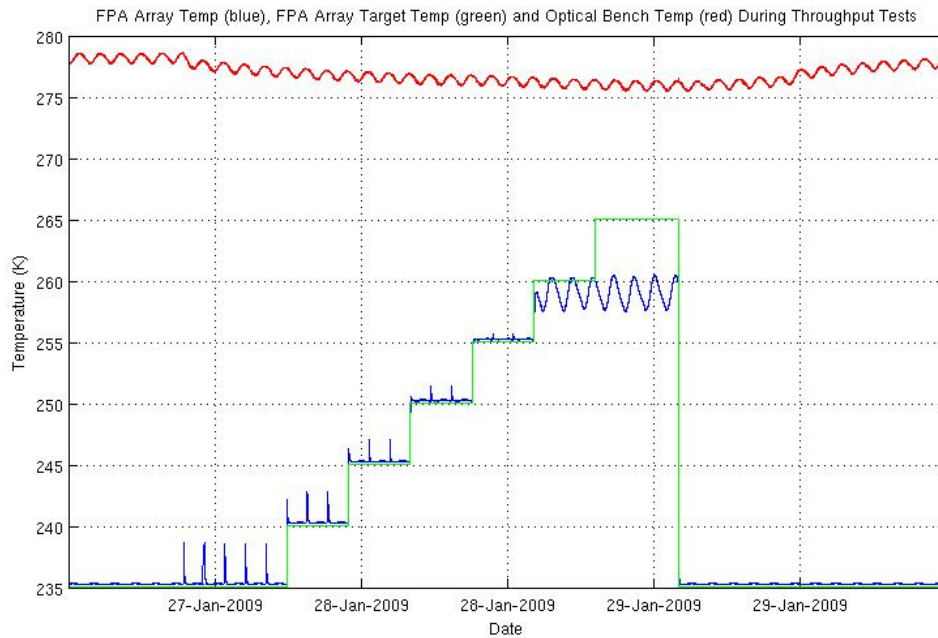


Figure 3-10: Temperature of the FPA (blue) compared to the temperature command (green) and optical bench temperature (red) during the first throughput test

Parallel to the FPA temperature increase, the optical bench temperature is decreasing. The temperature of the PMD detector changes from 232 K to 266 K after the change of mode (FlightLine to GroundLine) done at the beginning of the test.

The general evolution of the throughput during the test is **an instantaneous increase as a function of time (as thus of the temperature)**. On the other hand, this increase is spectrally dependant, with higher values in the UV. The recovery rates are listed in Table 3-4. The similar spectral behaviours are observed as well for the FPA as for the PMD.

Unlike after a switch-off, the FPA throughput comes back almost immediately to the pre-test level when the temperature is set back to the nominal value. No hysteresis can be seen.

Recovery rates			
Channels 1&2		Channels 3&4	
FPA	PMD	FPA	PMD
2.5 %/5K	2 %/5K	< 1 %/5K	< 1 %/5K

Table 3-4: Recovery rates measured thanks to the WLS and the SMR

This difference of behaviours between the test and a switch-off is illustrated on Figure 3-11. The throughput at 330 nm is plotted according to time between January and March 2009. The first spike corresponds to the throughput test whereas the second one is the result of a switch-off. On the FPA plot the hysteresis after a switch-off is clearly seen while there is no

hysteresis after the test. This result is unexpected and requires further investigation to be explained.

One notable difference between the test and the instrument switch-off conditions, apart from the instrument optical bench temperatures, is a different setting of the Dale Resistor (survival heating system switch), which is off during the throughput test and set to on during switch-off periods.

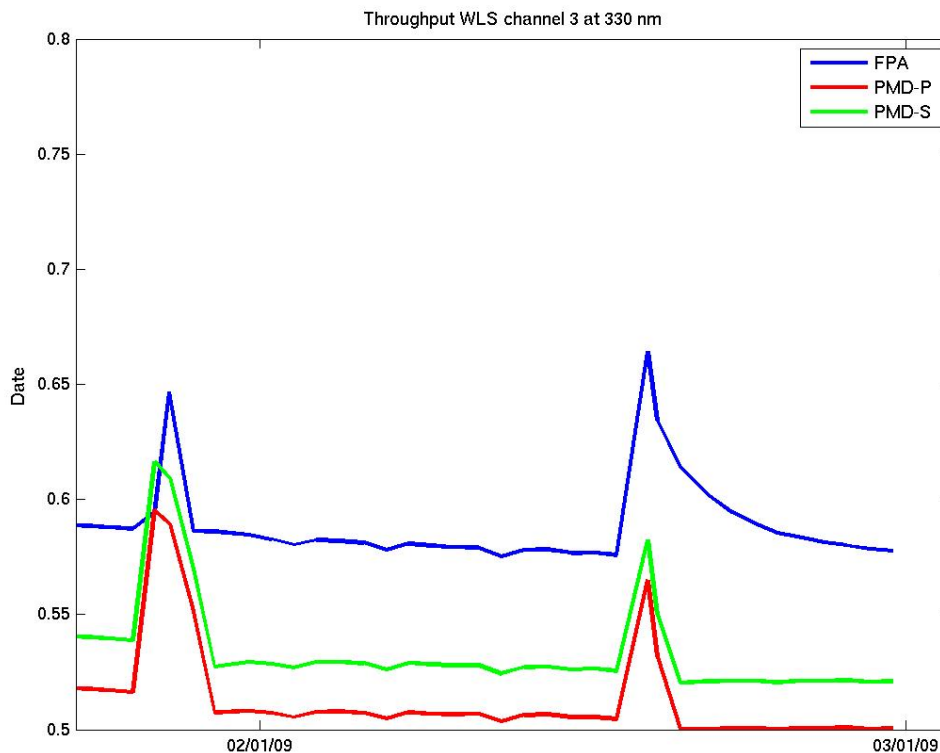


Figure 3-11: Throughput measured thanks to the WLS at 330 nm. The first spike corresponds to the first throughput test, the second one corresponds to a switch-off.

There has been no significant effect observed on the residual etalon before and after the first throughput test.

3.3.3 Second throughput test

To complement the first throughput test, a second test was performed between the 7th September and the 12th September 2009. It has been decided to set higher detector temperatures in order to be more representative of the switch-off conditions during the 1st part of test. It has also been decided to carry out a 2nd part tagged as “outgassing phase”, during which the detectors have been set to 305 K [RD9].

In order to reach higher detector temperatures, the Peltier coolers were used in heating mode.

3.3.3.1 Experimental protocol

During the second throughput test, the temperature of the FPA is increased first from 235 K to 270 K. Then, 300 K is reached thanks to 5 K steps. Next, a 14 orbit long plateau at 280 K is set. Finally, a decontamination period at 305 K is tested for around 30 orbits (2 days). The FPA temperature profile is plotted on Figure 3-12.

During the whole test period, the PMD Peltier coolers are set to GroundLine mode.

3.3.3.2 Observations

During the first incremental phase, the throughput increases proportionally to the temperature as during the first throughput test with a similar growth rate.

From **285 K** onwards the increase rate per temperature as observed during the 1st throughput test (see before) for the FPA slows down and even a decrease of the throughput is then observed. This temperature is the temperature since which the FPA are warmer than the optical bench. They are thus no longer the coldest parts of the optical path. During the plateau at 280 K (at 09/09) a small decrease in signal is noted. The decrease is still noted during the out-gassing phase at 305 K superimposed to the immediate proportional response to the temperature variation.

The PMD do not show such behaviour: the throughput increased at the beginning of the test when the coolers were set to ground line mode. Then the throughput follows the slightly decreasing temperature of the PMD (resulting from the decreasing temperature of the optical bench) and comes back to previous levels after the test.

Figure 3-12 shows the throughput variation at two different wavelengths as well as the FPA temperature profile during the test. The additional decrease is well seen.

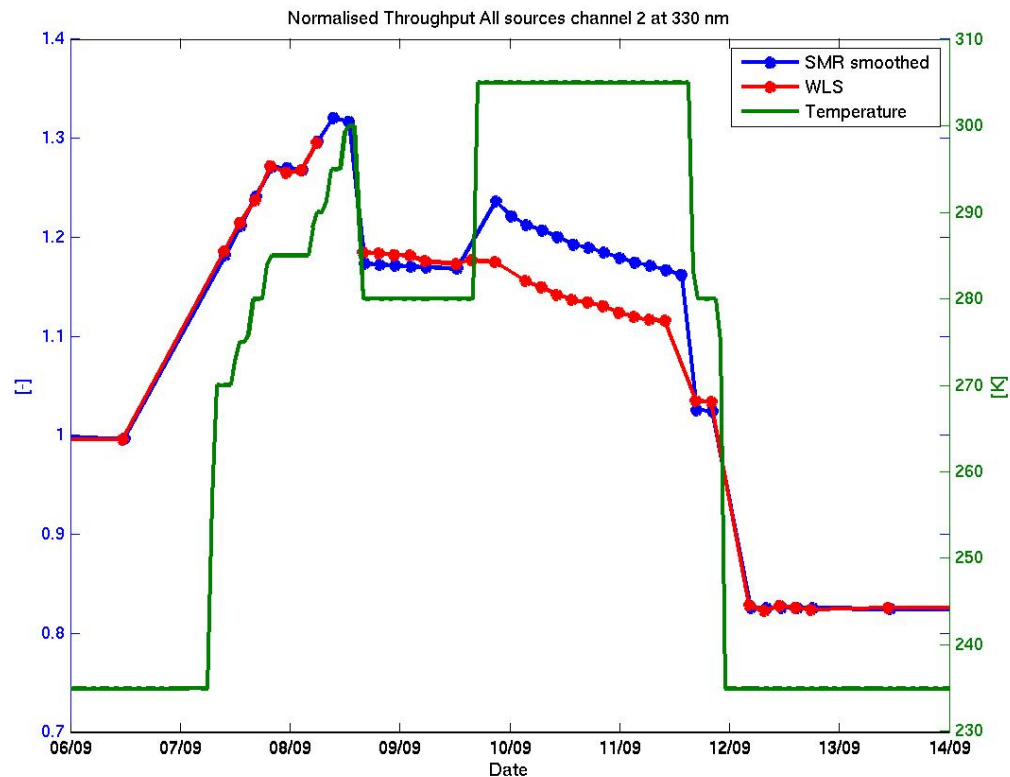


Figure 3-12: Throughput and FPA temperature evolution during the 2nd throughput test at 330 nm. Up to 5 WLS spectra depending on channel could not be processed during the course of the 8th of September.

To sum up, **the proportionality between the throughput and the detector temperature is observed, as for the first test, but with an additional continuous decrease initiated around 285 K during the 7th of September for the FPA.** At the end of the test, when the temperature of the detectors is set back to its nominal value, the throughput of the FPA has decreased compared to the pre-test level. **An additional decrease of 25 % in the UV and 10 % in the visible has to be deployed** (the reference level corresponds to January 2007). **The throughput of the PMD after the test corresponds to what was expected** knowing the pre-test level and the “normal” degradation rate.

The differences between WLS and SMR measurement during the outgassing phase for various wavelength are not yet fully understood, but may be related to significant different integration times (long integration times for WLS and short integration times for SMR) introducing large error bars on the WLS dark current offset at this high temperature.

Figure 3-13 shows the ratio of the **LED measurements** between before and after the test. The ratio is expected to be the same for all the channels because the same wavelength of 570 nm is emitted just in front of each detector. A significant difference is observed: for example, channel 1 seems to experience a 3 % improvement of the throughput whereas channel 3 shows a loss of 5 %. Moreover the results of the LED measurements are quite different from

those of the other light sources which show a consistent loss of throughput after the test whatever the channel is. It can be noted that the inter-channel differences for the LED measurements increased with time during the test.

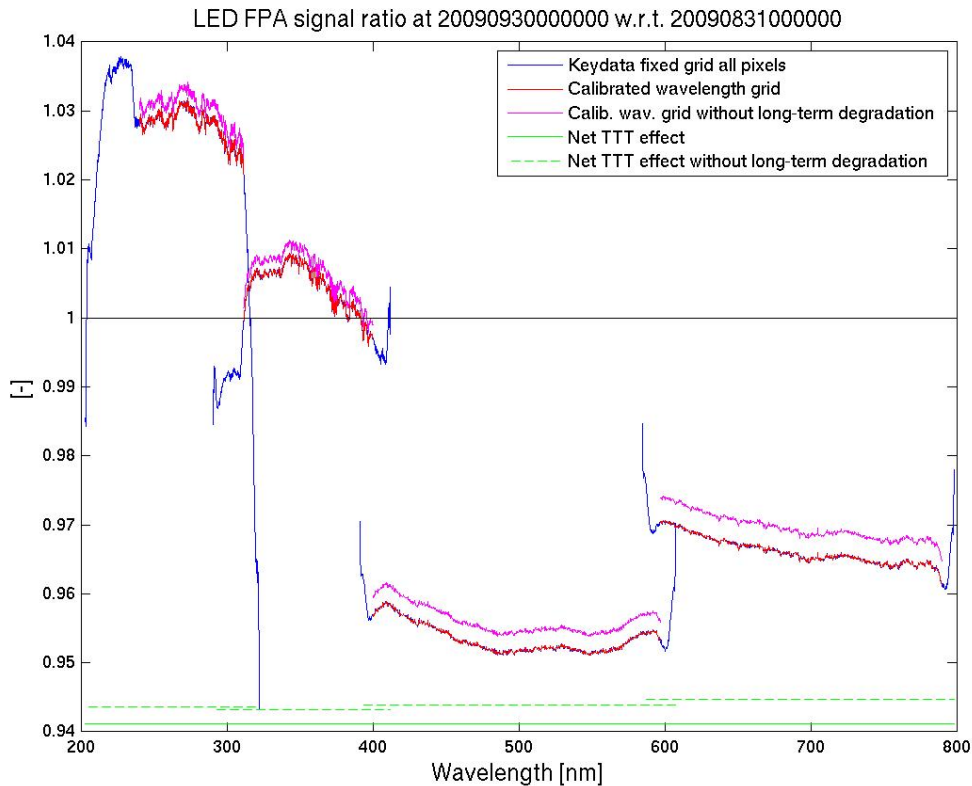


Figure 3-13: Ratio between the LED throughput measurements (after/before)

The net effect for all the detectors (inter-channel sum of the improvement or loss) is also plotted on Figure 3-13. It is assumed that such calculation can be done since the LEDs are supposed to emit the same light whatever the channel is. The net effect is negative, even when the normal expected degradation is removed. The overall consequence of the second throughput test as observed at the LED level is (as for the other sources) a loss of throughput.

The impact of the second throughput test on the residual etalon is visible on Figure 3-7. A strong change can be observed (at 12/09/2009). The etalon shifts spectrally of about 3 nm. The residual etalon amplitude increases: the peak to peak amplitude after the test is about 4 times larger than it was before.

In order to investigate a potential signature of diffusion due to the built-up of contaminants during the test, the width of the spectral lines of the SLS after test has been compared to that before the test. No broadening is observed. Even if the test resulted in a significant loss of throughput, it seems to have no effect on the width of the lines.

A threshold seems to have been reached during this test around 285 K. Yet, it has to be noted that the maximum temperature of the FPA during the test was kept below the decontamination temperature defined in the operational manual at 311 K.

It is also interesting to notice that **since this second throughput test the throughput degradation slowed down**. Despite having engendered a significant throughput loss, the test seems also to have stabilised the degradation. This decrease of the throughput loss is visible on Figure 3-1, Figure 3-2, Figure 3-3 and Figure 3-4 keeping in mind that the test was performed from 07/09 to 12/09/2009.

Moreover, the throughput degradation rate of all sources with respect to the end of the throughput test has become similar to the one of the LED per channel as can be seen on Figure 3-14.

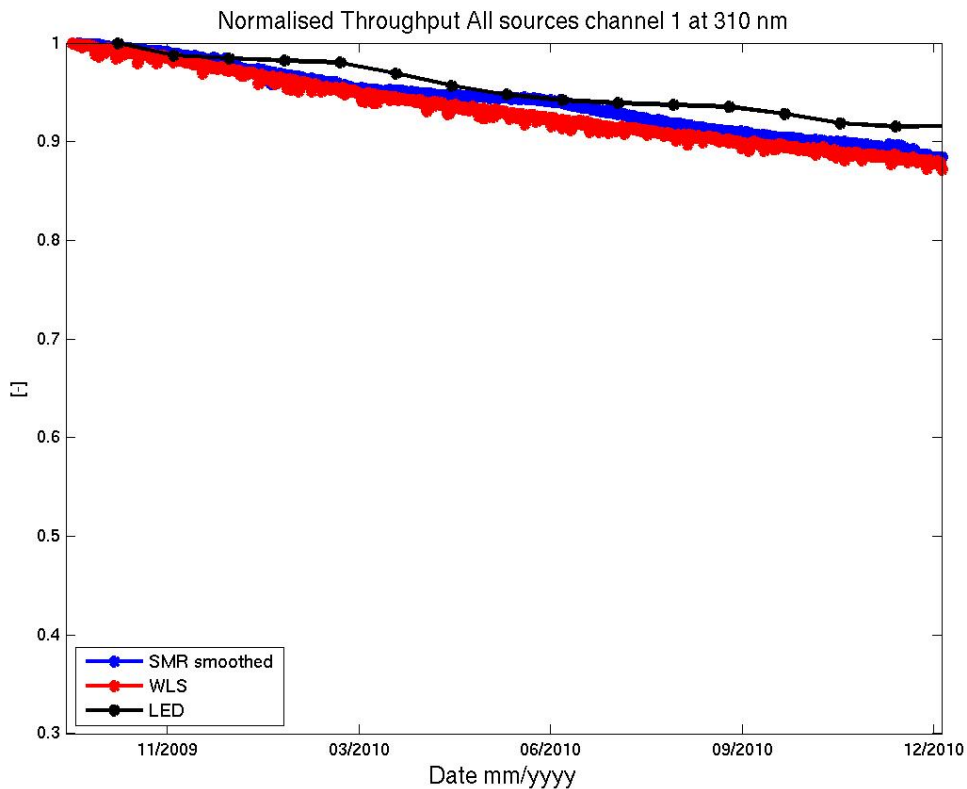


Figure 3-14: Throughput evolution at 310 nm since the second throughput test, relative to the throughput after the test

Table 10-1 in summarises the GOME-2 versus GOME-1 changes. The driving of each of them is addressed.

4 FACTS, OBSERVATIONS, INITIAL CONCLUSIONS

4.1 LED Records

The recordings with the LEDs have a very limited amount of optical elements behind the LEDs: two lenses, well protected in the “barrels” (channel objective), one flat window at the entrance of the Focal Plane Assemblies, and the detector proper.

All LEDs emit at 570 nm.

Fig. 3.3 gives the comparison of signal measurement time series for **different sources at the LED wavelength**. It shows that the degradation at this wavelength is strongest for the LED. From that one can conclude that the LEDs degrade under space conditions. The time series of LED signals show a decrease in signal by about 7-8 %/year up to the end of 2010. There is some slight variation between the channels. (See Figs. 3.1 to 3.4, 3.5).

Also from OMI records it is known that LEDs degrade in their output under space conditions. One then can assume that the observed long-term trend is due to a degradation of the LEDs, not of the FPAs/PMDs. However, for short-term observations, as e. g. in the TT1 and TT2 campaigns, the data from LEDs provide valid information.

4.2 White Light Source versus Sun Records

The time series of the measurements with the white light source (WLS) and the smoothed records of the daily sun measurements via the diffuser show a degradation which is different between these two sources.

The light paths for these two observations are common to 95%: only some few elements in the calibration unit are different, and they happen at slightly different scan mirror positions.

The signal recorded for the WLS is systematically lower than the one for the sun measurements. One therefore could conclude that the difference comes from a degradation of the WLS. This degradation has a spectral weighting and is not the same at all wavelengths.

The envisaged mechanism for this degradation lies in the functioning of the halogen cycle inside the lamp. On ground, this is driven by convective transport due to the significant thermal gradients inside the bulb. This convective mechanism does not work in the weightlessness of space, causing a deposition of filament material on the cooler walls of the bulb and reducing output in this way.

Fig. 4.1 shows the lamp degradation spectrum obtained in this way.

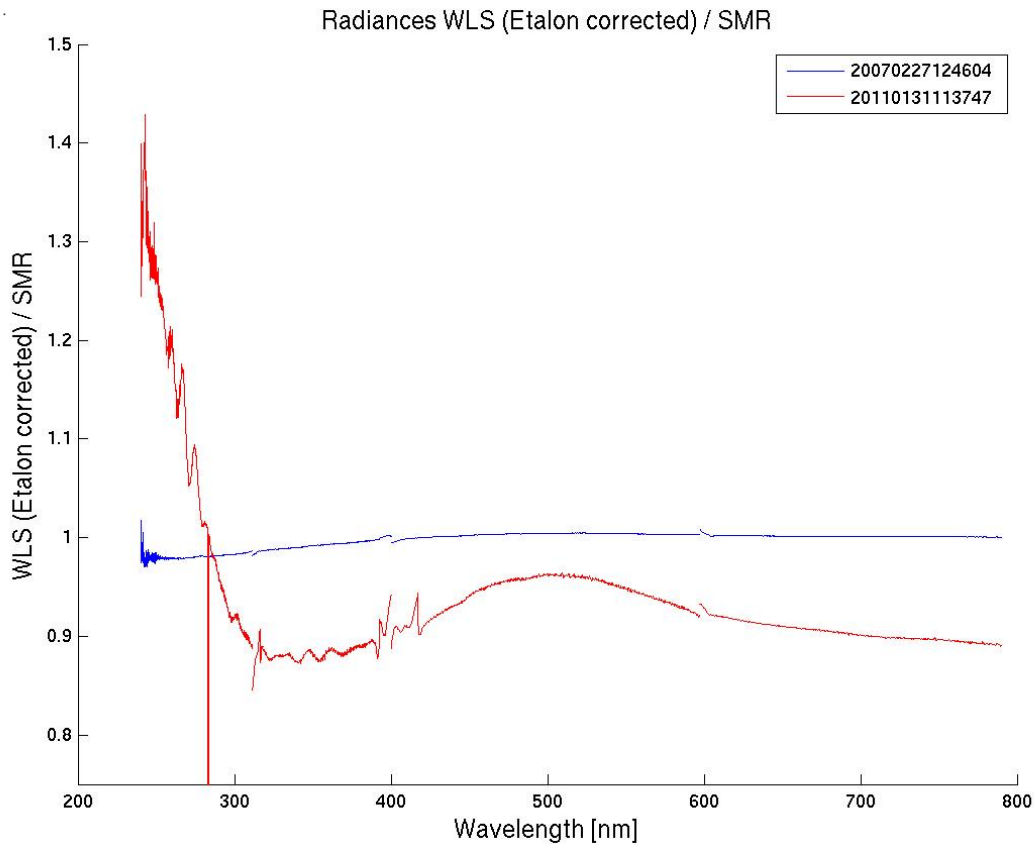


Fig. 4.1: WLS degradation spectrum : ratio WLS signal to sun signal, BOL/now

One should keep in mind that the WLS was not intended as a radiometric calibration source but was embarked to enable Etalon correction for the data!

4.3 Scan Mirror Degradation

The Earthshine recordings show systematic differences in the levels for East, Centre, and West pixels. This was already observed on GOME 1.

From these measurements, confirmed by assessment of the polarisation behaviour, SRON has been able to model a deposit (of unspecified nature) on the scan mirror of 8 nm thickness (period not specified). This results in a UV throughput degradation of ca. 15 % (period not specified).

From GOME 1 to GOME 2, the nature and thickness of the coating on the scan mirror had been changed. Observed deposition rate on GOME 1 was about 10 nm/year. The temperature on the scan mirror could not be measured; the temperature on GOME 1 which carried a temperature sensor was within +/- 0.3 degree of the optical bench temperature. One can assume that the conditions on GOME 2 are very similar.

The technical note concerning the scan mirror deposit modelling is attached as Annex 1. Fig. 4.2 recalls the spectral characteristics of the scan mirror contribution (period not specified)

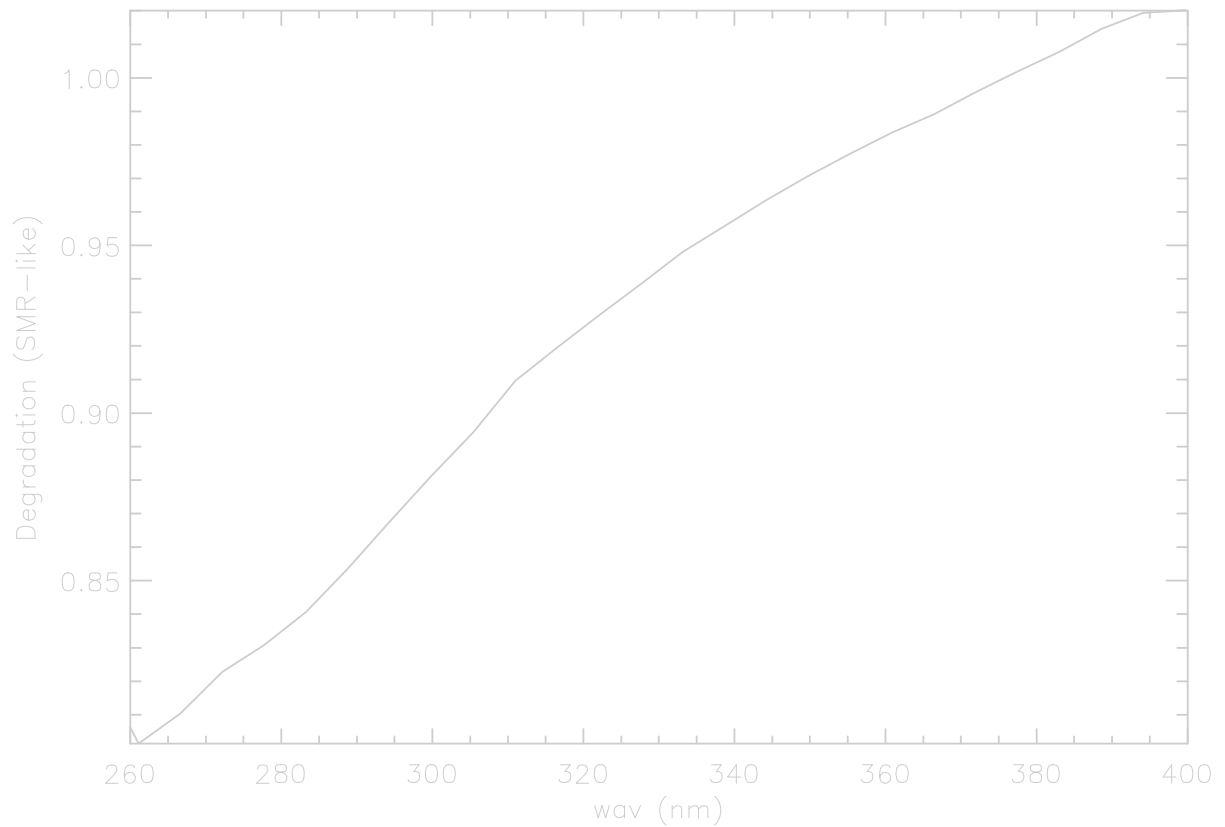


Fig. 4.2: Scan mirror degradation contribution (period not specified) with a generic 10 nm deposit. (Apologees for the poor plot quality)

5 DEDUCED PROPERTIES OF A DEPOSIT

From what was said before, we can conclude that there is some material which is deposited

- in the FPAs on the cooled detectors
- in the cooled (to a slightly different level) PMDs
- on the scan mirror (not necessarily the same, but possibly)
- possibly on the general optics.

We then can try to establish some criteria with which this deposit has to comply:

1. The deposit exists and grows at temperatures around – 38 deg C, possibly as well at temperatures of 5 deg C (optical bench/scan mirror temperature).
2. The deposit has a strong absorption in the UV, reducing rather monotonously towards the VIS/NIR, with a possible bump at around 370 nm.
3. The deposit exists both in the FPAs and in the PMDs, although probably in different amounts.
4. When heated to 310 K = 23 deg C, the deposit evaporates (at least partially). This rules out any polymerisation on the detectors.
5. The source material must be available in sufficient amounts.
6. It has to have a supply rate which is slow enough to act over a long time (years!)
7. It has to be available within the optical bench enclosure: an inward migration of the necessary amounts can be ruled out.
8. **It has to be different to GOME 1 to explain the different degradation rate by a factor of 3 – 5: either a new material, or one applied in a different process, or one available in different amounts!**

6 FINDING THE CANDIDATE MATERIAL

Many candidate effects have been discussed and discarded:

- collection of water vapour e. g. from MLI, desorption from the Alodine coating of the optical bench and its elements, even from the CFRP body of the Metop platform. Initially the prime suspect, eventually it was ruled out for thermodynamical reasons (at the prevailing pressure levels and temperatures, water ice would sublime and not form a lasting deposit. This was demonstrated in a principle test setup with cooled detectors and water injected into the TV chamber: even at a pressure level of few torr, no ice deposit would form on the detectors.) Also, the spectral features of the degradation could not be explained with a water deposit.

- radiation effects on the optics: too small dose for the rad hard material, no dynamics in TT2
- radiation effects on the detectors: too small dose, no credible dynamics during TT2 (a small increase in leakage current is observed and is to be expected!)
- thermomechanical effects/optical distortions: spectral and temporal behaviour
- outgassing of FPA materials (Stycast, O-ring): dynamical, spectral behaviour, not different to GOME 1

Eventually, one candidate material was singled out in the assessment process: the conformal coating material used on the charge amplifier and proximity electronic boards on the optical bench.

(To be clear: this does not concern the conformal coatings on the boards of the CDHU, Scan Unit Drive Electronics, and CU Power supply!)

From the declared materials list, the material was identified as Arathane® 5750-A/B (LV), a material of the polyurethane family. This material is allowed for use in space projects and in general compliant with the limits set for product outgassing. It had been used on GOME 1 as well.

In order to demonstrate the general viability of this candidate material, a test was prepared in the ESTEC Materials Lab. The setup and results of the test are provided in Annex 2.

With the identified candidate and the additional information provided by the test, one now can check whether the criteria established in the previous chapter are matched by the candidate material:

	Criterion	Compliance
1	Condensable @ -38 deg	Yes, demonstrated by test
2	Strong UV absorption, roll-off to the VIS/NIR	Yes, see attached spectrum 1)
3	Both in FPAs and PMDs	Possible from thermal and topographic conditions

	Criterion	Compliance
4	Re-evaporation at 300 K	Not demonstrated but likely
5	Sufficient amount	Estimated to be 50 – 70 g in the Optical Bench Enclosure

6	Supply dynamics	Outgassing of conformal coatings is a long term process, depending on - curing method -bake-out time and temperature - operational temperature -accommodation: size of venting hole, venting volume, pressure difference
7	Within the OBE	yes
8	Difference to GOME 1	Yes, see footnote below 2)

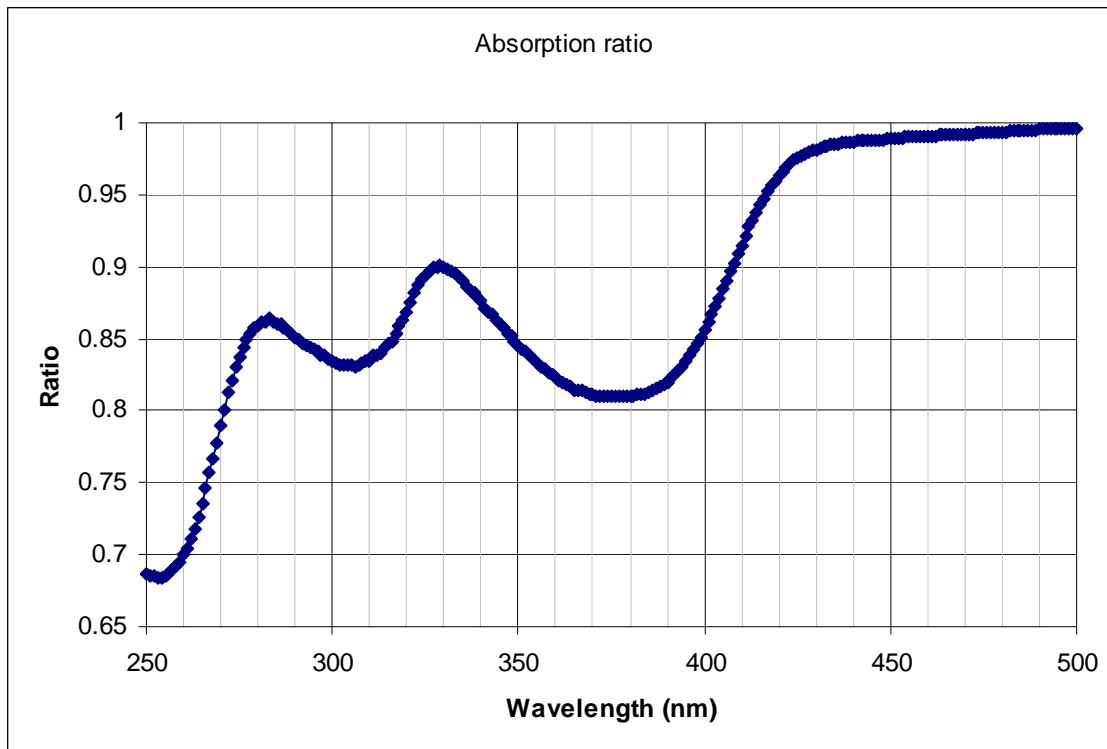


Fig. 6.1: Spectrum of outgassing products:

The reported spectrum corresponds to 660 nm of collected deposit on a sample plate at – 38 deg C. (For full report see Annex 2)

2) Differences GOME1/GOME 2: On GOME 1, the only PCBs with conformal coating within the optical bench enclosure were the charge amplifier boards at the backside of the FPAs, with an estimated board area of $38.5 \text{ cm}^2 \times 4 = 154 \text{ cm}^2$.

On GOME 2, there are the two additional PCBs of the charge amplifier boards of the PMDs, plus the boards of the 6 proximity electronics of $17 \times 8 \text{ cm}^2$, hence a total board area of 1047 cm^2 . This corresponds to a PCB area ratio GOME 2/ GOME 1 of 6.8!

7 BUILDING THE HYPOTHESIS

In order to generate a scenario which can explain all the different observations it is necessary first to understand how the different compartments of the instrument and its environment are connected. This is presented in the next subchapter 4.1 The Spaces Involved.

Each of these spaces has its own size, temperature, and partial pressure. To get a feeling for the conditions which lead to the observed behaviour of the spectral data, a model of the conditions and flows will be described in the subchapter 4,2 Steady State Hypothesis.

7.1 The Spaces Involved

Within the GOME 2 instrument, one has to distinguish a number of individual volumes which are interconnected but all have their special environment in terms of volume, temperature, contaminant partial pressure, and connectivity to other volumes. These individual compartments will in the following be described one by one. They are:

- the detector compartments of the FPAs
- the detector compartments of the PMDs
- the electronic compartments of FPAs and PMDs
- the proximity electronics
- the optical bench enclosure
- the outside electronics
- the satellite environment.

The Detector compartments of the FPAs are hermetically sealed volumes which house the detector and the Peltier elements which provide the closed-loop thermal control for the detectors, normally at -38 deg C. They are unchanged in design, parts, materials, and processes from GOME 1. The individual FPAs are all slightly different in that the tilt angle of the detector w. r. t. the optical axis is dependent on the wavelength range covered by the channel concerned.

Fig. 7.1.1. shows a cross section through an FPA. The detector compartments have a tube (normal to the plane of the cross section, hence not shown). With this tube, they are connected via a flexible metal bellows pipe to a 2-1 manifold. 2 FPAs each are connected to one manifold, the two outlets of the manifolds are then again connected to a third manifold thus bringing together all four FPAs. From the third manifold, a stainless steel pipe with an outer diameter of 6 mm leads through the rim of the optical bench bottom and ends up in a 20 mm standard flange.

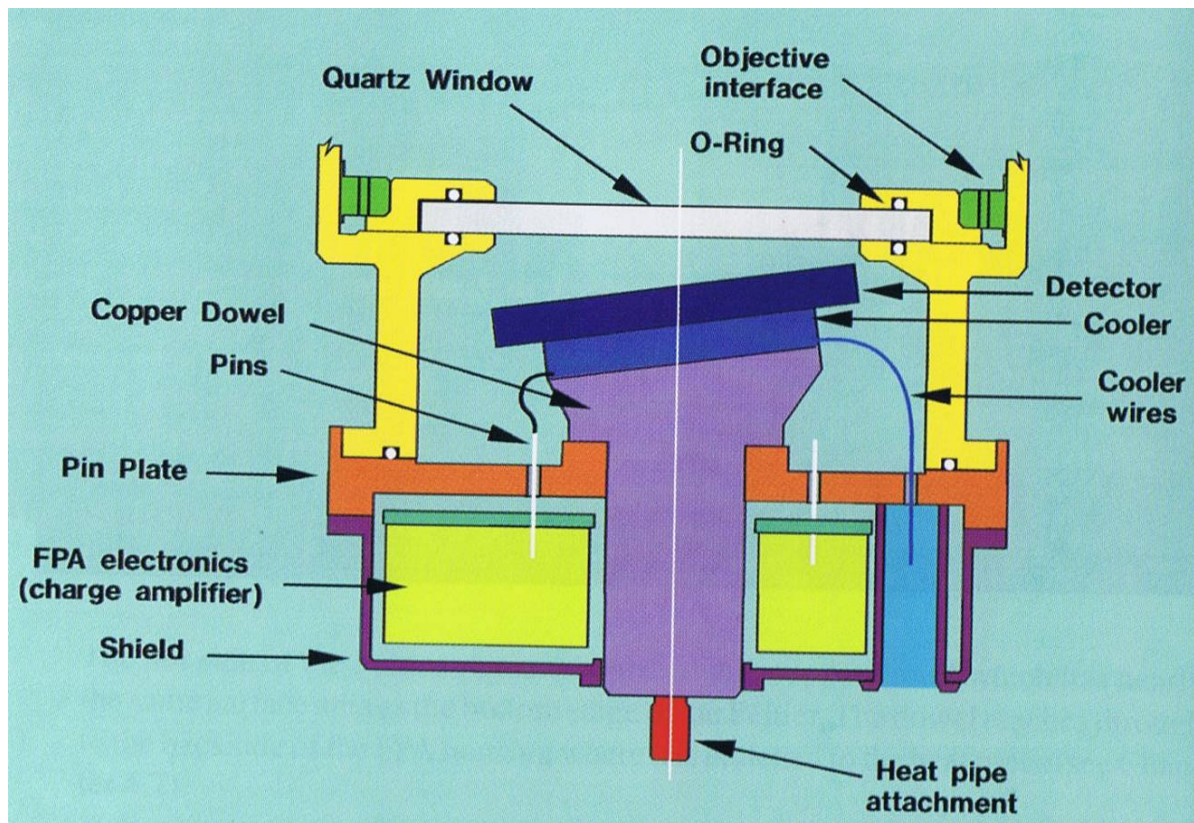


Fig. 7.1.1: Schematic cross section of an FPA

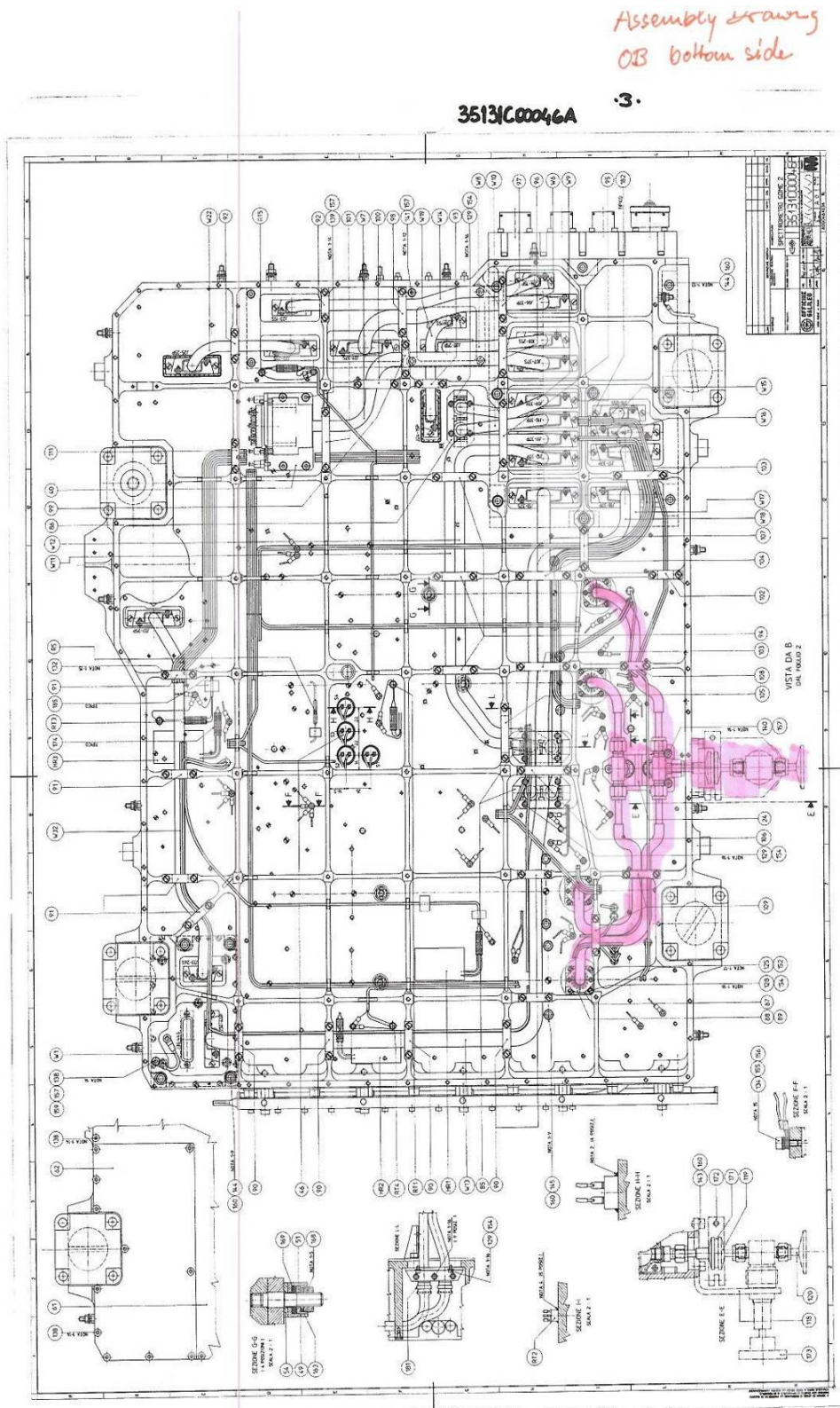


Fig. 7.1.3: Bottom view of the optical bench without EMC shield. The pipes of the FPA evacuation system are highlighted in pink.

During ground operations, the flange is connected via a valve to a pump system which evacuates the ensemble of FPAs.

When being readied for launch, the valve is removed, after the FPAs have been filled with dry nitrogen. The flange is then covered by a cap (Fig. 7.1.4) which connects the FPA pipe work back to the bottom part of the optical bench. Note that, contrary to previous statements, this cap had already been used on GOME 1.



Fig. 7.1.4: Cap covering the flange of the evacuation system during launch and in orbit

The detector compartments of the PMDs are similar in design to the FPAs, only the mechanical shape is different due to accommodation constraints.

However, there are two important differences to the FPAs:

- the Peltier coolers are driven “open loop” to an equilibrium temperature of about – 38 deg C (hence similar to the PFA detector temperature but with less stability) but operationally they are less flexible (no heating possible to heat to pre-set temperature)
- the PMDs are not evacuated during ground operations, but just have venting holes into the optical bench enclosure. These venting holes are 4.5 mm in diameter.

Apart from the mechanical parts, all other parts, materials, and processes employed are the same as used for the FPAs.

The electronic compartments of FPAs and PMDs are accommodated at the backside of the sealed pin plates. They carry the charge amplifiers, the first amplifications stage for the detectors. These boards have a diameter of about 7 cm. The electronic compartments of FPAs and PMDs are vented via venting holes of 4.5 mm into the optical bench enclosure.

The Proximity electronics forms the second stage of signal amplification/conditioning and the A/D conversion. It is, for each channel individually, accommodated in a rectangular box which is mounted on top of each channel objective (“barrel”). The board size of each of these proximity electronic boards is 17*8 cm. The boxes have no venting holes but have openings at the side where the harness is passed through; these openings have sizes of 160*28 mm, out of which at least one third can be considered as being free from wires.

Note that the proximity electronics is a new feature on GOME 2 and did not exist on GOME 1! On GOME 1 this functionality was accommodated in the CDHU. Motivation for this change was the need for a faster detector readout, in order to minimize aliasing effects.

Fig. 7.1.5 Proximity electronics mounted on top of the channel objective

The Optical Bench Enclosure (OBE) is the volume of the optical instrument proper. It comprises

- the optical bench, which accommodates all the optical elements with their structural support, the FPAs and PMDs, proximity electronics, and the interconnecting harness;
- the bottom compartment, which is formed by a rectangular pattern of ribs stiffening the optical bench. Through the ribs, with the according cutouts, the harness between optical bench and the electronic boxes is routed, as well as the pipe work of the FPA evacuation system. The bottom compartment is closed by a flat plate, the EMC shield. This closure is (EMC) tight but not vacuum tight;
- the cover, providing the “dark” volume for the optics. At the front towards the entrance of the light path, there is a labyrinth between optical bench and cover, in order to suppress stray light. The opening towards the space environment is estimated as $160 \times 28 \text{ mm}^2$.

Between top and bottom, both the pipe work and the harness with its connectors have to pass through. These holes are taped but of course not vacuum tight.

Fig. 7.1.6 Optical bench with optical elements

Fig. 7.1.7 Bottom side of optical bench

The outside electronic boxes, with much more substantial board area than what is present in the OBE, are the CDHU and the scan mirror drive electronics. They are both accommodated outside the OBE but close to it. The same holds for the Calibration Unit with the lamps and the sun diffuser and its protective shutter. Another small electronic box with the power supplies for the lamps is accommodated on top of the Calibration Unit.

All these electronic boxes vent through their venting holes into the space environment close to but outside the OBE.

The satellite environment: In the context of the GOME 2 degradation discussion the only point of interest here is the pressure environment: for big satellites like METOP or Envisat, one can assume a “pressure cloud” of a considerable size to surround the satellite. This is caused by

- outgassing of harnesses and electronic boxes
- outgassing (mainly water) of the multi layer insulation
- outgassing (mainly water) of the CFRP elements (on METOP in the service module)

The existence of such a cloud is proven by the need to regularly decontaminate instruments with cooled elements (e. g. IASI, SCIAMACHY, SEVIRI,...)

7.2 Steady State Hypothesis

Phenomena involving transport of material are frequently modelled as being in “steady state”. Such a model has three principal elements:

- (a) source(s)
- (a) sink(s)
- a reservoir

The sources for the contaminant deposit on the instrument are the conformal coatings on those PCBs which are accommodated within the OBE: the charge amplifier boards of the FPAs and PMDs, and the boards of the proximity electronics on top of the channel objectives.

The total mass of conformal coating on these boards has been estimated to be 50 – 70 g.

As active electronic circuitry (although not high power), the temperatures of these boards is higher than that of the passive mechanical and optical elements within the OBE. Still,

compared with e. g. power converters, the temperatures of these boards are pretty low. Therefore, the release of offgassing products from the polymeric coating material is slow.

The sinks are

- the cooled FPA detectors. Although the path to the detectors is with a high flow resistance, the very cold detectors (in comparison to the source temperature) present the cold spot to collect condensable material.
- The cooled PMD detectors, at a comparable temperature. Compared to the FPAs, they are much closer to the sources, with only the venting hole forming a flow resistance in the path.

These sinks are only “temporary sinks”: they act as sinks only as long as being cooled. If not cooled or even heated, they can act as temporary sources, with limited source strength.

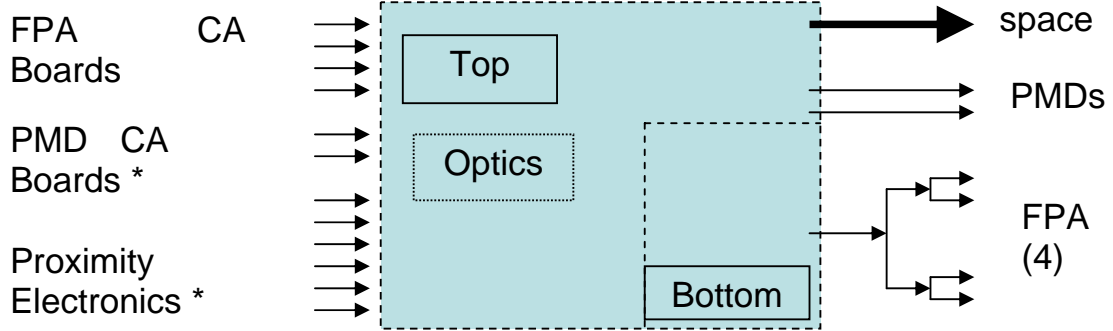
- the space environment, into which the majority of the material will be lost eventually. However, as said before, the pressure difference between inside and outside is not that substantial, because the satellite carries its molecular cloud around it. Hence there is no pressure induced flow but just molecular diffusion which is, a priori, a slow process. One also has to keep in mind that, close to the OBE, the GOME electronic boxes vent and release similar products from their conformal coating (of a slightly different nature because of different products being used there) as is released within the optical bench.

The reservoir is presented by the optical bench enclosure, and everything contained in it. All these elements are at a temperature of about 5 deg C (see Fig. 3.9, red curve), so well below the source temperatures.

If it acts as a reservoir with a residence time defined by the balance between sources and sinks, it has as a consequence that **the contaminant is ubiquitous within the optical bench!** Even if some places are more remote and have a considerable flow resistance for material to get there: we talk about days and weeks and months and years!

As a final remark in this context it has to be stated that the level of the steady state is not a constant. At any point in time it will be a balance between what is released by the sources and by what is lost to the sinks, and both will change with time. But this will be a slow change and impossible to quantify.

Steady State



Sources

Reservoir

*New w. r. t. GOME 1

Fig. 7.2.1. Steady state diagram

8. DISCUSSION

From all the previous observations and considerations, the hypothesis to explain the observed degradation of the GOME 2 instrument and the difference in behaviour to GOME 1 and other instruments looks as follows:

The prime source of the problem is the Arathane conformal coating which is used in various places within the optical bench enclosure. This coating releases volatile products, which then deposit onto the optical elements, the cooled detectors, and probably the scan mirror. This material had been used already in GOME 1, where as well a degradation of the optical throughput was observed. The difference to GOME 1 is that in GOME 2, the board surface area has increased by a factor of more than 6, with accordingly more coating amount to act as source for the offgassing products.

The starting point of the hypothesis has been confirmed by a test performed in ESTEC's materials lab, which confirmed

- the release of volatile products from the conformal coating material
- the condensation of the volatile products at a temperature of -38°C
- the principle spectral features as observed in the degradation: strong UV absorption, a bump at $\sim 370\text{nm}$, roll-off of the absorption towards the IR end of the spectrum.

However, there are a number of observations which do not fit or contradict each other. These will be discussed in the following.

8.1 Spectral features

The most representative spectrum of the throughput degradation is the one from the smoothed sun spectrum (Fig. 8.1)

It shows

- a strong absorption in the UV
- a bump at 370 nm
- a rather flat levelling-off towards the long wavelength end.

The Arathane spectrum, if compared to that, is rather similar but with one marked difference: it shows two spectral peaks rather than only one!

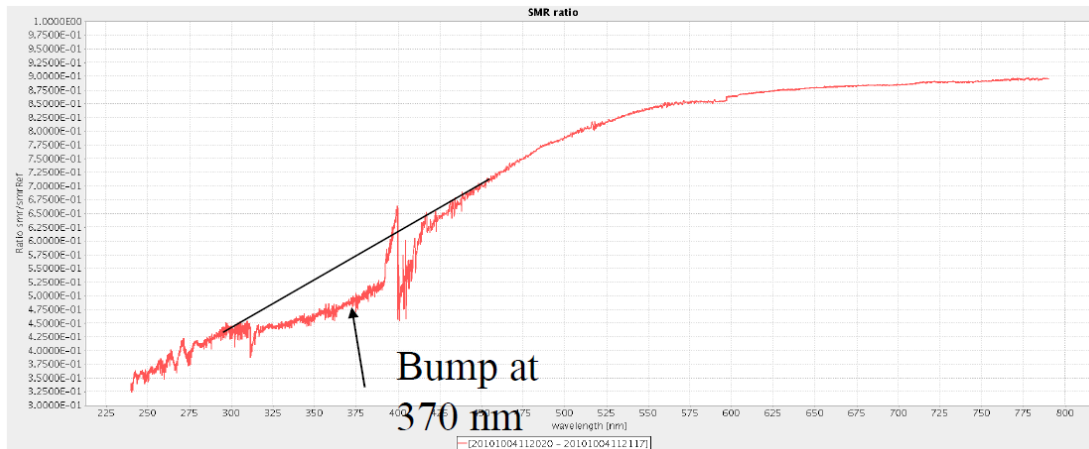


Fig. 8.1: Ratio of smoothed sun spectrum Oct. 2010 to first sun spectrum recorded after launch

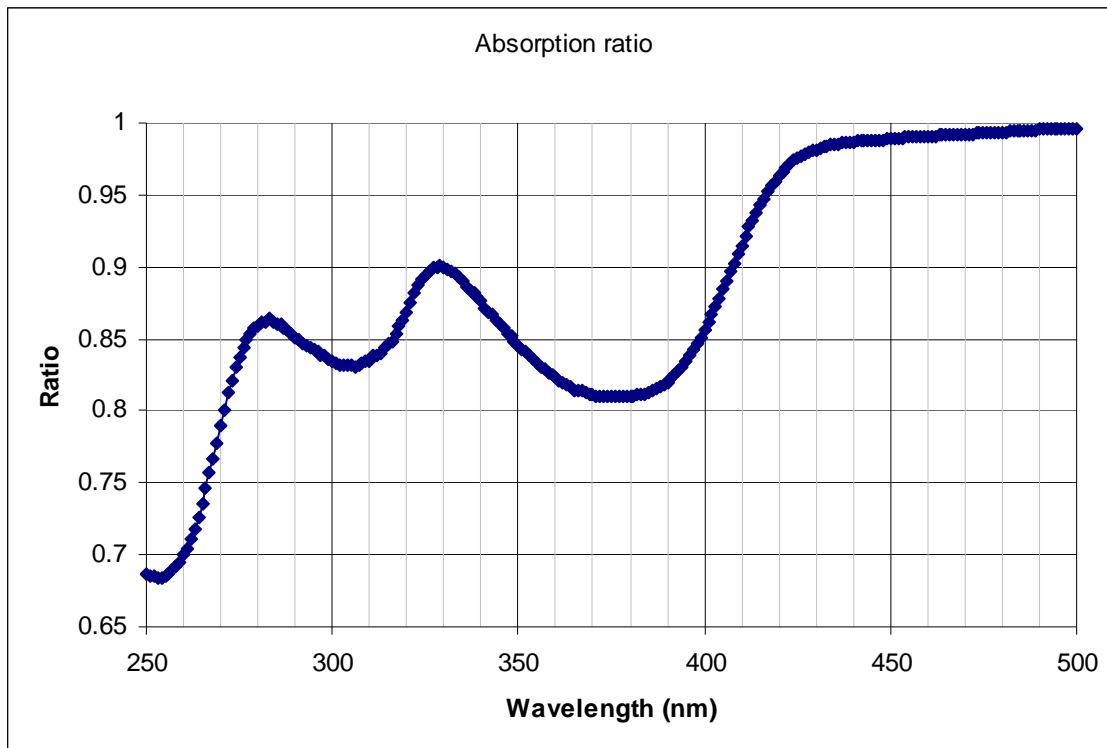


Fig. 8.2: Spectrum of offgassing products from ESTEC test

From the test campaign done in the ESTEC materials lab it is known that the collected offgassing products are a mixture of several components, out of which two are significant in terms of amount (Table 8. 1, marked with arrows):

Peak	Retention Time	Area	% Total
N-(o-Tolyl)ethanolamine	27.102	1007655494	1.57
N-Phenylglycine	27.241	1005799539	1.57
5-Methyl-3-phenyl-1,3-oxazolidine	27.385	626865435	0.98
Tetraethyl pyrophosphate	28.986	593369378	0.93
N-propyl-benzenamine	29.334	519323377	0.81
N-Methyl-2-(N-phenylacetamido)acetamide	31.207	30478883315	47.58
Aromatic Amine	33.456	12477468789	19.48
Phthalic acid or Phthalate isomer	33.531	584290087	0.91
Not identified	33.625	846842572	1.32
Not identified	33.839	770188233	1.20
Not identified	33.972	594105769	0.93
7-(diethylamino)-4-methyl-2H-1-Benzopyran-2-one	37.941	14558594604	22.73

Table 8.1: Result of GC-MS of the collected offgassing products

A third amount which is significant in terms of collected mass is a group of components and can be discarded here.

One can now assume that the two major collected components are the ones which generate the two peaks in the spectrum.

One significant difference between the ESTEC test and the real instrument is that for the instrument, all electronic boards and boxes have been baked out prior to integration into the instrument: no such procedure has been applied to the Arathane sample used in the ESTEC test. Therefore, the more volatile component could have been removed by this process, leaving only the less volatile to be released in orbit.

Speculating that the short-wave peak is caused by the more volatile component, the spectrum with this one removed then would look like the spectrum displayed in Fig. 8.3.

It has been discussed with the ESTEC Test Lab to verify this hypothesis by a modified test setup and conduct. Results are not available yet. Also, the Test Lab people would not exclude that the second peak is a “facility blank” and not a product of the offgassing process.

One then could even go as far as trying to put this speculation on a quantitative basis: the material collected in the ESTEC test has been quantified, by means of the QCM, as being 660 nm thick. If the relevant agent is the less volatile component, which amounts to 23 % of the collected material, then the absorption peak as per Fig. 8.3 would correspond to an equivalent layer thickness of 152 nm. If one compares the peak in the modified test spectrum (Fig. 8.3) with the peak in the sun spectrum (Fig. 8.1), **this would correspond to a layer thickness of about 88 nm of the less volatile component. With a typical refractive index of organic components of 1.45, this would create an additional optical path length of nearly 130 nm.**

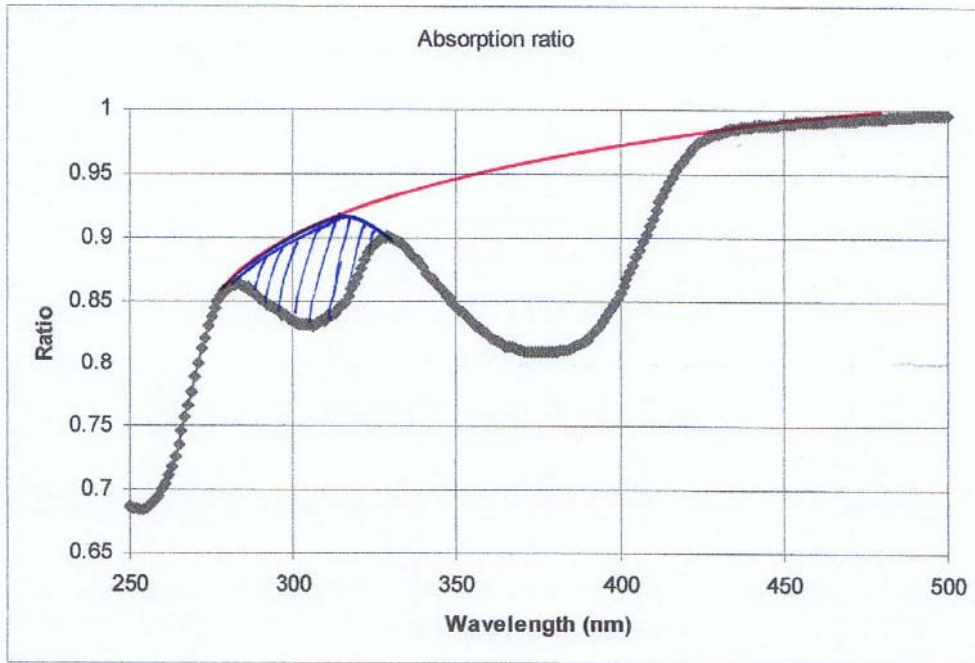


Fig. 8.3: Corrected spectrum with only one major absorbing component.

8.2 Temperature dependence of signal during TT1/TT2

Initially believed to be a processing artefact, the measurements performed during the different temperature plateaus set for the FPA detectors reveal a very systematic and reproducible pattern: every 5 deg. temperature increase leads to a signal increase by about 2.5 %, which is very steady between the commanded steps (Fig. 8.4).

This becomes even more obvious when comparing the signal change per temperature change as shown in Fig. 8.5.

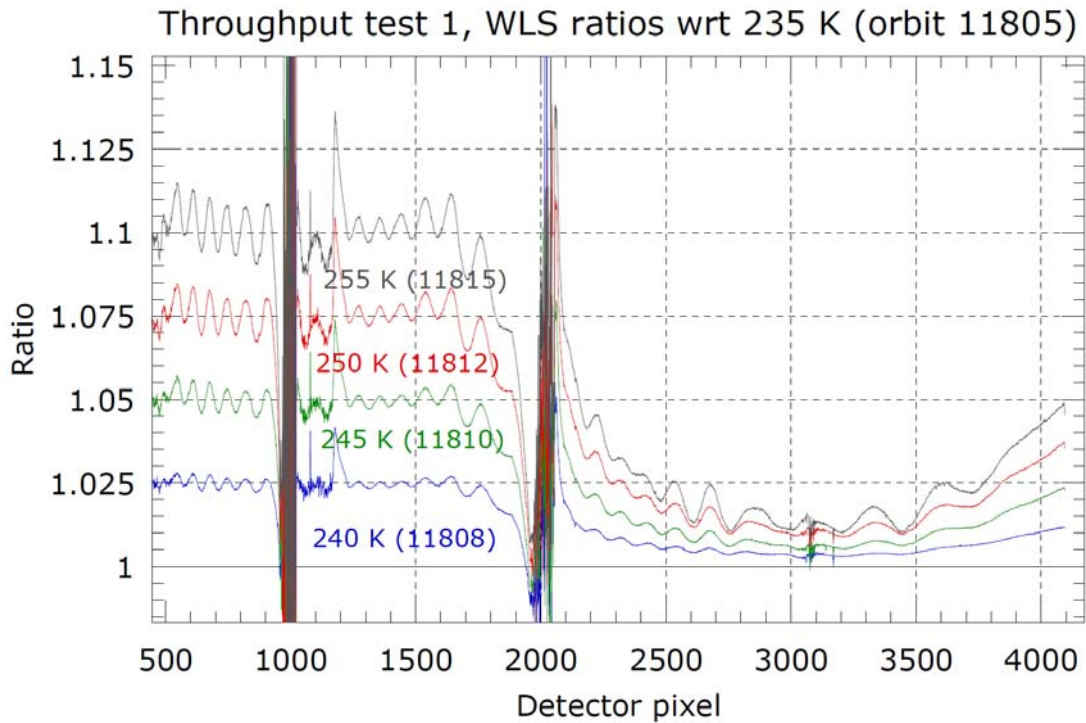


Fig. 8.4: WLS signal level ratios w. r. t. the level of 235 deg (nominal operational temperature)

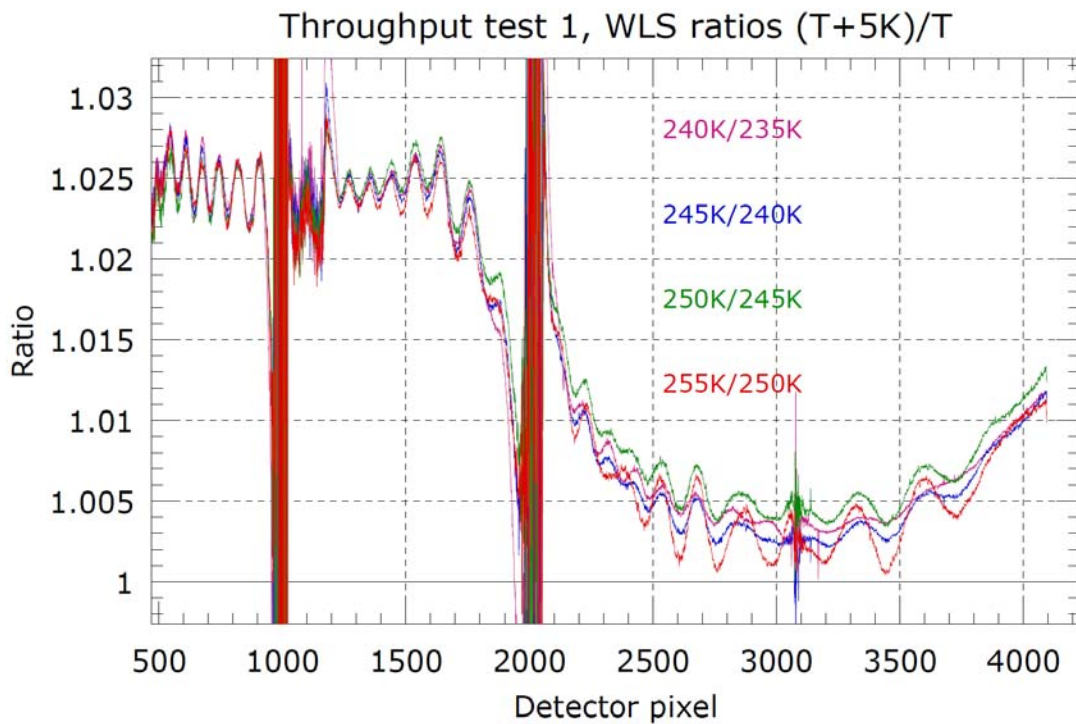


Fig. 8.5: same as above, but normalised to temperature step size (5 deg)

What we can see is a very reproducible pattern of signal change versus temperature step. In particular, the stability of the Etalon structures in channels 1 and 2 is remarkable. This very linear behaviour of signal change versus temperature suggests that the underlying cause is a physical temperature dependence (e. g. of the refractive index) rather than a thermodynamical effect: evaporation or similar transitions would follow an exponential behaviour rather than a linear one. However, from the equations of Fabry-Perot for the treatment of Etalons, if the refractive index alone would show such a linear temperature dependence, one would expect phase changes in the Etalon (all other conditions, like wavelengths, incidence angle etc. being the same).

There are indications that some temperature dependence of the signal has already been in place, with smaller effect though, at the beginning of the mission: when looking at the two temperature plateaus used in the IOV (i. e. “warm” detectors and nominal detector temperature), one can see already an effect few weeks after launch (Fig. 8.6)

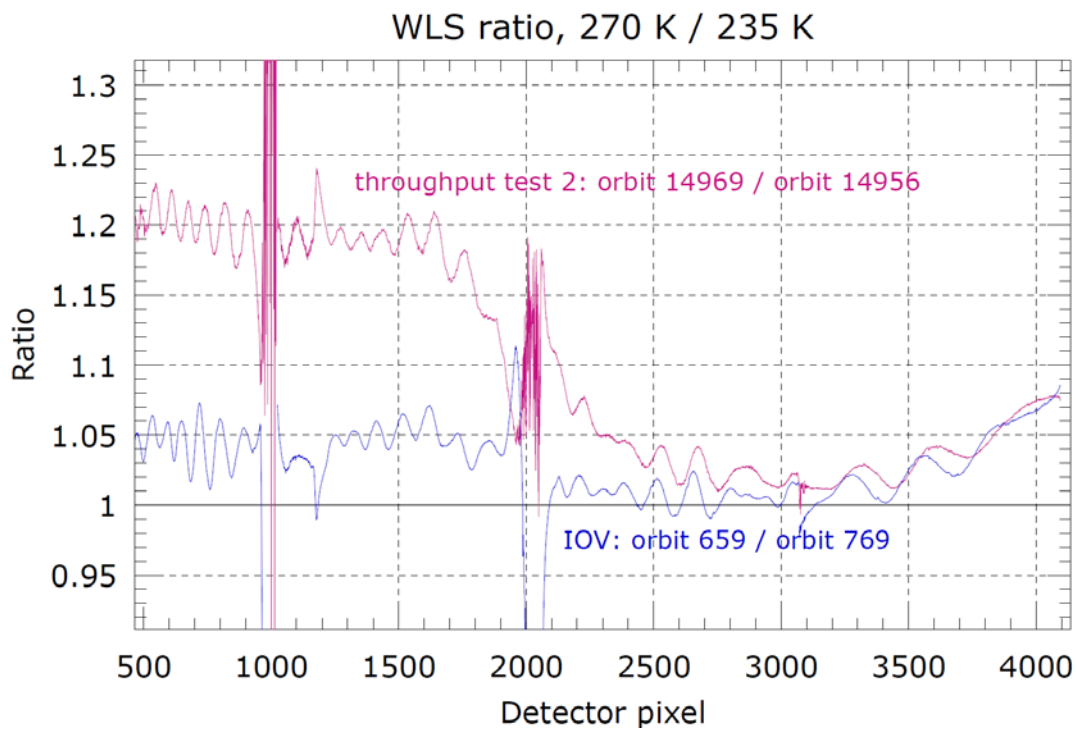


Fig. 8.6: Comparison temperature effects in IOV and TT2

Finally, when looking at broadband spectral features, one could by “visual low-pass filtering” come to a spectral interpretations as per Fig. 8.7, showing a inverse pattern to the observed absorption peak in the sun spectrum (Fig. 8.1) and the processed Arathane offgassing product spectrum (Fig. 8.3).

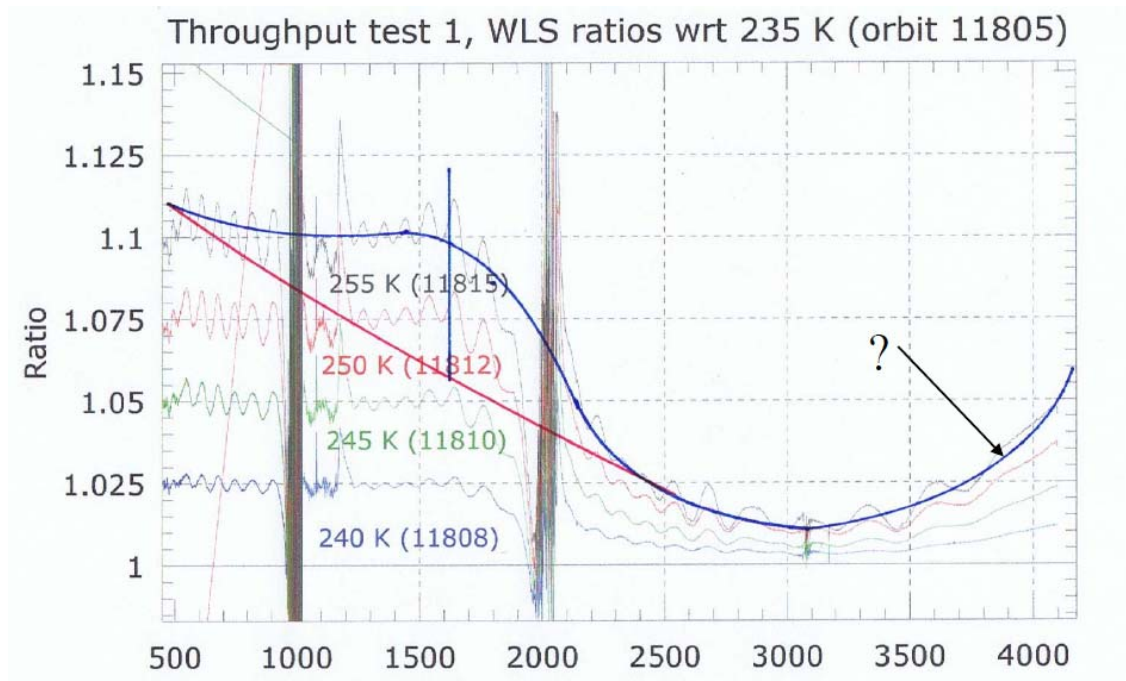


Fig. 8.7: Visual low pass filtered spectral behaviour

What however is different to all other spectral features is the increase towards the long-wavelength end, not observed in any other spectral recordings.

8.3 Evolution of the FWHM

Triggered by some observations made during the ongoing calibration campaign for the next flight unit of the GOME 2 instrument series, the in orbit behaviour of the slit function has been analysed by means of “well behaving” lines of the spectral calibration lamp.

The result of this analysis is shown in Fig. 8.8.

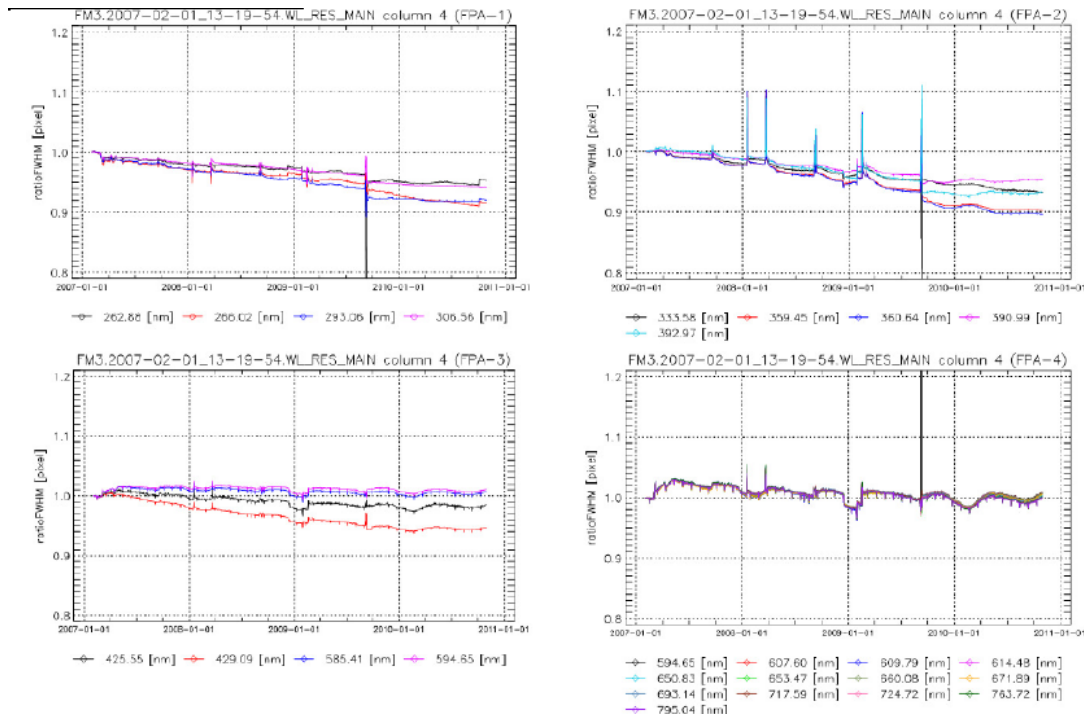


Fig. 8.8: Evolution of the Full Width Half Maximum of selected spectral lines

Ignoring some problems with the line stability/ processing limitations which cause steps in the time series, what one can observe is the following:

- the FWHM decreases with time
- the decrease is strong in channels 1, 2, and at the short wavelength end of channel 3
- the evolution shows a step function in channels 1 and 2 at the time of TT2
- the evolution shows a change in slope in channels 1 and 2 at the time of TT2.

All these features are as well observed in the general throughput evolution!

Hence, there seems to be a connection between the FWHM evolution with the overall instrument degradation.

THESE OBSERVATIONS CAN BE EXPLAINED AS FOLLOWS: SELEX GALILEO, IN PREPARING THE INSTRUMENT, HAVE ON PURPOSE SOMEWHAT DEFOCUSSED THE INSTRUMENT, IN ORDER TO IMPROVE THE SAMPLING OF THE SLIT WIDTH ON THE DETECTOR PIXELS. IF NOW, BY GRADUAL CONDENSATION OF OFFGASSING MATERIAL, AN ADDITIONAL OPTICAL PATH LENGTH OF APPROXIMATELY 130 NM IS CREATED, THIS IMPROVES THE FOCUSING, IF THE FOCUS IS IN FRONT OF THE REAL DETECTOR. IMPROVED FOCUSING, HOWEVER, MEANS NOTHING ELSE THAN A DECREASED FWHM OF SPECTRAL LINES. AS THE LAYER GROWTH DYNAMICS IS WHAT WE SEE IN THE GENERAL DEGRADATION, WE ALSO FIND IT BACK IN THE FWHM EVOLUTION.

9 SUMMARY AND CONCLUSIONS

We know that we have a number of elements within the GOME 2 instrument which degrade:

The LEDs

The white light source

The scan mirror

The detectors suffering (expected) radiation damage.

There are observations of the **temperature dependence** of the signal response of the detectors which are not in line with “normal” detector behaviour, and which have not been observed neither on the instrument prior to launch nor on the instrument which is now under testing. However, some of the effect seems already to be present shortly after launch in the IOV data. No real conclusive explanation can be provided, but this observation is not the main concern.

We further know that we have a **potential contamination source** within the instrument enclosure: the conformal coating applied to the PCBs of the detector charge amplifier and the proximity electronics boards. The board space, and with that the amount of coating, is more by a factor of 5 – 6 compared to what had been the case for GOME 1.

Quite a number of observations could be explained by offgassing products of this conformal coating creating a steady state atmosphere within the optical bench enclosure, and from there depositing onto the cooled detectors of FPAs and PMDs:

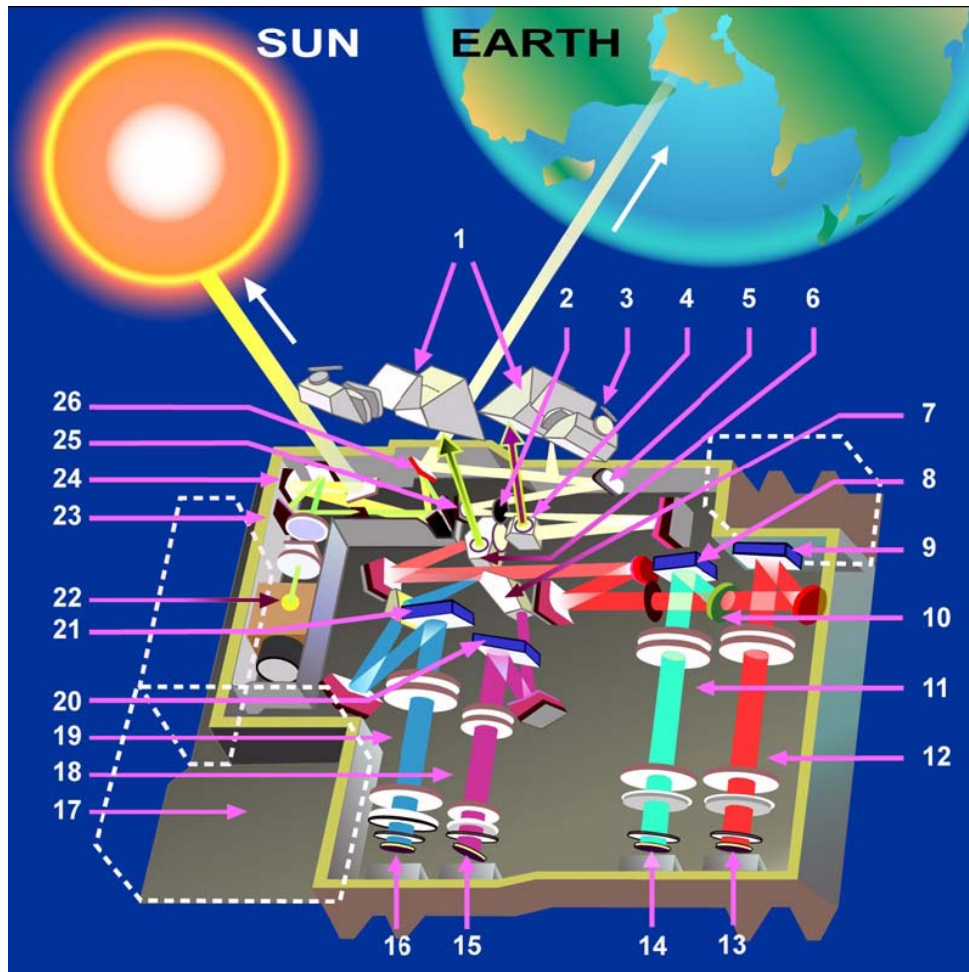
- in very general terms, the degradation is similar to GOME 1 but faster: this is compliant with a common root cause but different amounts.
- The spectral behaviour, with the additional speculation as per chapter 8.1 and considering the additional contribution of the scan mirror as per chapter 4. 3, is compliant with the observations, in particular the sun spectrum as displayed in Fig. 8.1
- The evolution of the Etalon structure, (Fig. 3-7), including the discontinuities at TT2
- The dynamic behaviour in TT2, in particular the step function within a short period of time (few orbits), can be logically only explained by material being removed from the detectors by the heating during TT2: no other instrument setting is changed during the test than the temperatures of the detectors.
- The difference in height and sign of this step function, varying between channels, can be interpreted as redistribution of deposit within the system of channels interconnected by the evacuation system.
- The change in degradation rate before/after the TT2,
- The difference in hysteresis observed between FPAs and PMDs after switch-off events,

- The evolution of the FWHM of spectral lines, showing the same dynamic features in their time behaviour as the general throughput degradation.

However, it should not be ignored that the migration path from the source (charge amplifier boards and proximity electronic boards) to the optical bench enclosure, to the bottom part of the OBE, through the rib structure, the cap installed before launch, the metal bellows pipes and the manifolds, and finally the rigid pipes to the FPA volume with the cooled detectors is a very long path with a high resistance. And this migration path is in competition with the much more direct path of losses through the instrument aperture to space.

N.B.: The fact that it has not been possible to model the stated layer thickness with thin film software might be due to the fact that inherently, thin film software assumes a collimated beam (as is e. g. the case for the scan mirror) but not a focussed beam (even if slightly defocused) as we encounter in the FPAs.

10. Appendix



1 - Dispenser	10 - Beam splitter	19 - Channel # 2
2 - Calibration Slit	11 - Channel # 3	20 - Grating # 1
3 - Detector	12 - Channel # 4	21 - Grating # 2
4 - Double Brewster Prism	13 - 590 - 790 nm	22 - Calibration lamp
5 - Telescope mirror	14 - 401 - 600 nm	23 - Calibration Unit
6 - Predispenser Prism	15 - 240 - 315 nm	24 - Sun diffuser
7 - Channel Separator	16 - 311 - 403 nm	25 - Telescope mirrors
8 - Grating # 3	17 - Electronics box	26 - Scan mirror
9 - Grating # 4	18 - Channel # 1	

Artist Impression of the GOME-2 Optical Layout (courtesy of ESA)

Subsystem/Item	Driving consideration	Remarks/explanation
Structure		
Overall dimension in z-direction	METOP panel size	Desire to stay on one panel (distortions AIT advantage)
Overall dimension	Need to accommodate PMD	Still enveloped by radiator size, so no significant change
Foot location	Optimum suspension of optical bench w.r.t. vibration	METOP vibration loads (rms) approx. 2 times higher than ERS
Optical bench/cover I/F	AIT	Cover (as well as all other subsystems) can be removed without the need to remove any other S7S except EMC shield/harness
Cover		Topography to accommodate new PU
Cover/CU I/F	EMC requirements	Redesigned to provide light-and EMC tightness
Thermal		
New radiator surface	Need for add. Radiators because of somewhat increased dissipation, worse environment, different dissipation topography	Basic concept maintained: -passive for the main instrument -active cooling loop with Peltiers and heat pipes for detector cooling -safe mode heaters and Dale resistor
Scan Unit		
Scan Unit Mechanical Assembly		
Wireless resolver	Removal of potential single point failure	Angular transducer based upon the same principle as for GOME-1 but without flexible electrical connection between rotor and stator
Scan mirror heater	Suppressed as result of the above	Never used on GOME-1
Gap between housing and axis	Debris confinement	PDR result

Subsystem/Item	Driving consideration	Remarks/explanation
Scan Unit Electrical Assembly		
Microprocessor	Obsolescence of previous type	
µP periphery	SU/CDHU protocol, new functions	Resulting from CDHU change (CDHU is now an ICU, SU considered as secondary processor incl. Full patch and dump functionality)
Max scan angle	Science	Double swath w.r.t. GOME-1
Scan profile	Science, torque optimisation	Both old and new profile implemented
Continuous rotation	Scanner performance	Enabled by deletion of flex connection
Calibration Unit		
Sun FOV	METOP orbit	
Additional white light source	Science	Qualified in ENVISAT/SCIAMACHY
Wavelength calibration lamp modification	Science	Additional spectral lines by changing gas fill from Ne to 10% Ar/90% Ne
Deletion of power supply	Power distribut. architecture	
GOME Power Distribution Unit		
New Unit	Power distribut. architecture	Additional lamp to be supplied in CU, higher voltage for WCL, separate power busses ICU/equipment, noise immunity of FPAs/PU

Subsystem/Item	Driving consideration	Remarks/explanation
Command and Data Handling Unit		
	METOP electrical interfaces	In GOME-1, "DDHU" was secondary to ATSR DEU; i.e. DDHU had no ICU functionality
RBI interface	Own OBDH bus interface	
FMU interface	Own FMU interface	Data formatted according to CCSDS, incl. datation and packet primary/secondary, approx. 10-fold increase of data rate
Power interface	Separate ICU and equ. Power bus	Separate busses were not available for GOME-1
Secondary processor	Separation of ICU and scientific tasks	
FPA/PU interface	Noise immunity	Transfer from FPA/PU is now digital, not analogue
Box dimensions	Accommodation of all necessary boards	Compact size to be still compatible with an accommodation on the optical bench
Internal wiring	Minimise cabling errors	Double mother board
Flap	PROM exchange	Access to PROM for late exchange w/o need to remove box
Focal Plane Assemblies		
Mechanical layout	Noise immunity	Additional boards on top of FPA, now include DDDI filter and ADC
Peltier element	Optimisation of raggedness	Optimised TEC design provides more mechanical raggedness at same performance
Electrical layout	Noise immunity	Result of breadboarding
Readout speed	science	Double w.r.t. GOME-1
Polarisation Unit (new design)		
Array detectors	Science	15 bands instead of 3
Channels	Science	Both S and P instead of only P
Detector cooling	Science	To maintain sufficient signal-to-noise
Optics		To provide the coupling of light from the main beam, spectral dispersion and focussing
Housing	To accommodate channel S	Completely reviewed
Spectrometer		
Slit	FOV overlap main/PU	Changed from 10x0.10mm to 9.6x0.20mm

Subsystem/Item	Driving consideration	Remarks/explanation
	channels	
Predisperser	Coupling of PU channels	
Coatings	Vacuum stability	New coating specs/verification for optimal stability in vacuum
Dichroic filter	Vacuum stability	New filter specs/verification for optimal stability in vacuum
Grating substrate	Straylight minimisation	
Alignment lenses	Optimise alignment for in-orbit situation	

Table 10-1: GOME-1 to GOME-2 changes summary (from [RD6])